Supplementary Information (SI) for ChemComm.
This journal is © The Royal Society of Chemistry 2024

Supporting Information

Multifunctional Luminogens with Synergy of Aggregation-Induced Delayed Fluorescence, Two-Photon Absorption and Photocurrent Generation

Abhijit Chatterjee,[a†] Sundaravalli Narayanan,[a†] Sachin Thorat,[ab] Ajay J. Malik,[c] Madan D. Ambhore,[d] Aswini Narayanan,[ef] Anil Kumar Sihag,[a] Sukumaran Santhosh Babu,[ef] Mayurika Lahiri,[c] and Partha Hazra*[a]

[a]*Department of Chemistry, Indian Institute of Science Education and Research (IISER), Pune (411008), Maharashtra, India*

[b]*Innovation Campus Mumbai, BASF Chemicals India Pvt. Ltd., Plot No. 12, TTC Area, Thane Belapur Road, Turbhe, Navi Mumbai, 400705 (India), Maharashtra, India*

[c]*Department of Biology, Indian Institute of Science Education and Research (IISER), Pune (411008), Maharashtra, India*

[d]*Department of Chemistry, Yeshwant Mahavidyalaya Nanded, Nanded, PIN-431602, Maharashtra, India*

[e]*Organic Chemistry Division, National Chemical Laboratory (CSIR-NCL), Dr Homi Bhabha Road, Pune-411 008, India*

[f] *Academy of Scientific and Innovative Research (AcSIR), Ghaziabad-201 002, India*

* Corresponding author. E-mail: p.hazra@iiserpune.ac.in. Tel.: +91-20-2590-8077; Fax: +91-20-2589 9790.

Table of contents

Instrumentation:

Data characterization using ^{1}H NMR (at 300 MHz) and ^{13}C NMR (at 75 MHz) of all the final compounds are performed using Bruker Avance™ II NMR spectrometer with deuterated dimethylsulphoxide (DMSO-d_6) as solvent (having residual dimethylsulphoxide, 0.1%) and tetramethylsilane (TMS) as the internal standard. Chemical shift (δ) values are measured in ppm relative to DMSO resonance at δ = 2.54 ppm for ^{1}H NMR and at δ = 40.45 ppm for ^{13}C NMR. High-resolution mass spectra (HRMS) for all the compounds are recorded using ESI TOF in Water's SYNAPT G2 mass spectrometer. HPLC measurements were carried out using Water's Acquity-H Class UPLC with a UV detector (Agilent eclipse plus-C18 RRHD column). The injection volume is 0.5 μL and the flow rate is kept at 0.5 mL/min.

Single-crystal diffraction analysis data were collected at 100 K with a BRUKER KAPPA APEX II CCD Duo diffractometer (operated at 1500 W power: 50 kV, 30 mA) using graphite monochromatic Mo Kα radiation (λ = 0.71073 Å). The structures were solved by direct methods and refined by least-squares against F2 utilizing the software packages SHELXL-2017,[1a,b], and WINGX.[2] More information on crystal structures can also be obtained from the Cambridge Crystallographic Data Centre under the CCDC deposition number.

Steady-state solution-based absorption spectra are recorded on Shimadzu, UV-2600 UV spectrophotometer. Steady-state emission spectra and time-gated emission spectra of all the samples in solution and solid state are carried out using Fluoromax-4C spectrofluorimeter and Fluorolog-3 phosphorimeter (HORIBA), respectively. All the PLQY values mentioned in the manuscript have been obtained by a direct method (absolute quantum yield measurement) using an integrating sphere (Horiba K-sphere).

Time-resolved PL decay profiles have been recorded by Time-Correlated Single Photon Counting (TCSPC) and Multi-Channel Scanning (MCS) methods either using a diode-laser

source (375 nm, for a total time window of < 50 μs) or a spectra LED source (357 nm) in HORIBA Scientific instrument. The data was fitted with the help of DAS6 Fluorescence Decay Analysis Software from HORIBA by examining χ2-values and visually inspecting residuals where the fit with χ2 = (1-1.2) value is taken as the best fit.

For the two-photon absorption experiment, an 800 nm mode-locked Ti-Sapphire laser (Mai-Tai, Spectra Physics) excitation source was focussed onto the sample. Leica multiphoton microscope (Germany) was utilized for the two-photon cell imaging at 63X oil immersion objective.

Materials:

For synthesis purposes, all the important starting materials like triphenylamine, phosphoryl chloride, phthalic anhydride and ethyl (4-nitrophenyl)acetate were purchased from Sigma-Aldrich and were used without any further purification. For spectroscopic studies in solution, spectroscopic grade solvents were purchased from Spectrochem. Pvt. Ltd. India. For solid-state emission studies, crystals or powdered samples were held in between two quartz slides from TED PELLA INC.

Experimental Section

Density Functional Theory (DFT) calculation:

Quantum chemical calculations are performed using the Gaussian 09 program[3] using a high-performance cluster facility provided by IISER Pune. Initially, geometry optimization of all the luminogens is carried out in the solution phase (THF) using the IEFPCM method and the nature of the stationary point (minima on the PE surface) is confirmed by frequency analysis[4-5] at the B3LYP/6-31G (d,p) level. Furthermore, TD-DFT calculations are carried out for excited state geometry optimisation (S_1 state) using TD-SCF method at the B3LYP/6-31G (d, p) level of theory after obtaining a frequency-analyzed ground state optimized structure at

the same level of theory. For potential energy surface construction, a relaxed scanning has been performed along the donor-acceptor dihedral angle with a difference of 2° for a total of 20 steps.

QM/MM Calculations:

The quantum mechanics/molecular mechanics (QM/MM) model was built based on the single crystal structure and was utilized to analyze the electronic properties of the active QM molecule embedded in the aggregated crystal state. The surrounding molecules were defined as a rigid MM component to simulate the effect of a solid-state environment.[6] The high layer for QM was computed using the TD-DFT method of B3LYP/6-31G (d, p) level, and the low layer for MM is described by the universal force field (UFF)[7] augmented by Coulomb interactions which are in accordance with the quantum method. The monomer was configured to a high layer for QM calculated by the TD-DFT method of B3LYP/6-31G (d, p) level.

Preparation of neat films:

To prepare neat films, 0.5 mg of each luminogen is dissolved in 1 ml of spectroscopic-grade THF solvent. The solution is then drop-cast onto a clean quartz substrate and dried under reduced pressure for at least one hour to eliminate any solvent trapped within the film layer.

Cell culture and drug treatments:

HeLa cells were a generous gift from Dr. Sorab Dalal (ACTREC, India). The cells were maintained in 35 mm dishes (VWR, USA) and grown in Dulbecco's Modified Eagle Medium (DMEM; HiMedia, India) containing 4.5g/L Glucose and supplemented with 10% heat-inactivated FBS (Thermo Scientific, USA) and 1X Pen-Strep antibiotics (Thermo Scientific, USA) and incubated at 37°C in a humidified incubator with 5% CO_2 (Eppendorf, GmbH).

For the MTT cell viability assay, 10,000 HeLa cells per well were seeded in a 96-well plate (Eppendorf, Gm) and incubated at 37°C with 5% CO_2 for 18 hours post-seeding. Cells were treated with different concentrations of the compounds TN, TA, and TP or DMSO control (5µM, 10µM, and 15µM). 24 hrs post-treatment, drug-containing media was removed, and 100 µL of DMEM containing 0.5 mg/ml MTT (HiMedia, India) was added to each well and incubated at 37ºC in the dark for four hours. Post incubation, the MTT-DMEM solution was aspirated, and the purple MTT-formazan crystals were solubilized in 100 µL of DMSO and incubated for 15 mins in the dark before recording absorbance. The absorbance was recorded at 570 nm using the EnVision Nexus Multimode plate reader (Revvity, USA).

For multiphoton imaging experiments, $0.15x10^6$ HeLa cells were seeded on coverslips (pre-washed with 95% EtOH) in a 35 mm culture dish (VWR, USA) and incubated at 37°C with 5% CO_2 for 18 hrs. Cells were then treated with 10 µM of compound (TN, TA, and TP) and incubated for 24 hrs. Post-treatment, cells are washed twice with 1X DPBS and fixed with 4% formaldehyde for 20 minutes in the dark. After fixation, cells were again washed with PBS and mounted onto slides. The cells were imaged on a multiphoton confocal microscope at an excitation wavelength of 820 nm (Leica, Germany) and observed with a 63X oil immersion objective.

Detailed procedure for photo-current generation:

Here, the photocurrent generation experiment was performed in chronoamperometry mode, where current was measured as a function of time at a fixed potential of 0.9 V. A three-electrode configuration was used for the photocurrent measurement, where the working electrode comprising the target compound was drop-casted onto a FTO substrate. The Ag/AgCl electrode functioned as the reference, and another FTO plate was employed as the counter electrode. 0.2M sodium sulphate solution is used as electrolyte. Here the working electrode was prepared

by dissolving 1 mg of the compound in 0.5 mL of chloroform, followed by dropcasting the resultant solution onto the surface of an FTO plate.

Synthesis and characterization procedures

Synthetic scheme:

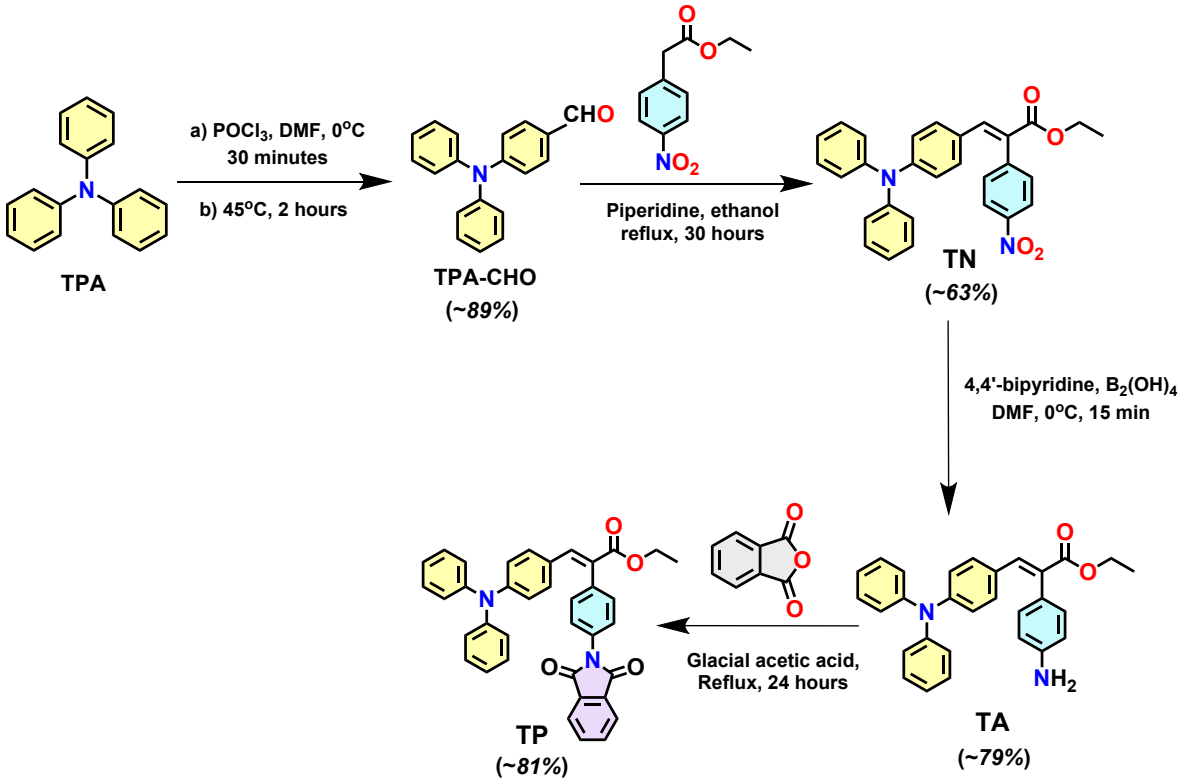

Scheme S1: Synthetic route of the designed compounds

Synthesis of TPA-CHO:

Triphenylamine (4 g, 16 mmol, 1 equiv.) was dissolved in dry DMF (17.8 mL) in a round bottom flask under a nitrogen atmosphere and the solution was cooled at 0˚C with continuous stirring. Phosphoryl Chloride (7.6 mL, 82 mmol, 5.13 equiv.) was added to the solution dropwise and stirred at 0˚C for 30 minutes. The reaction mixture was cooled to room temperature and kept under stirring for an hour. It was then heated to 45˚C and allowed to proceed for two more hours after which the crude product was poured into ice water and neutralized with aq. NaOH (10 g/ 100 ml). The light-yellow precipitate obtained is purified by column chromatography and characterized by ^{1}H NMR, ^{13}C NMR, and HRMS techniques (4.46 g, 89% yield).[8]

^{1}H NMR (400 MHz, $CDCl_3$): δ in ppm 9.81 (s,1H), 7.76–7.62 (m, 2H), 7.34 (dd, J= 10.4, 5.4 Hz, 4H), 7.22-7.12 (m, 6H), 7.01 (t, J= 8.9 Hz, 2H)

^{13}C NMR (100 MHz, $CDCl_3$): δ in ppm 190.56, 153.45, 146.23, 131.41, 129.83, 129.29, 129.16, 126.41, 125.21, 124.24, 119.42

HRMS (ESI): calc. for $[(C_{19}H_{15}NO)H]$ $(M+H)^+$ 274.1232, measured 274.1237.

Synthesis of TN:

To a stirred solution of TPA-CHO (3 g, 10.98 mmol) and ethyl 2-(4-nitrophenyl)acetate (2.52 g, 12.08 mmol) in ethanol (30 mL) at 25°C was added with piperidine (1.62 ml, 16.48 mmol) and stirred at 120°C for 30 hours. After the consumption of the starting material, the reaction mixture was evaporated. The product was obtained as a mixture of (E) and (Z) isomers in the ratio of 4:1. Therefore, the mixture is separated by preparative HPLC to afford the pure E-isomer TN as a yellow solid, which is characterized by ^{1}H NMR, ^{13}C NMR and HRMS techniques (3.2 g, 63 % yield).

^{1}H NMR (300 MHz, DMSO-d_6): δ in ppm 8.25 (d, *J* = 8.7 Hz, 2H), 7.78 (s, 1H), 7.57 – 7.43 (m, 2H), 7.33 (dd, *J* = 8.4, 7.4 Hz, 4H), 7.21 – 7.07 (m, 2H), 7.07 – 7.01 (m, 4H), 6.97 – 6.87 (m, 2H), 6.71 – 6.62 (m, 2H), 4.17 (q, *J* = 7.0 Hz, 2H), 1.19 (t, *J* = 7.1 Hz, 3H)

^{13}C NMR (75 MHz, DMSO-d_6): δ in ppm 166.60, 149.29, 147.40, 146.41, 144.25, 140.94, 132.58, 131.62, 130.30, 127.78, 126.10, 125.10, 124.36, 119.94, 61.31, 14.62

HRMS (ESI): calc. for $[C_{29}H_{24}N_2O_4]$ $(M)^+$ 464.1736, measured 464.1737.

Synthesis of TA:

To a stirred solution of TN (3.0 g, 6.46 mmol) in DMF (15 mL) at 0°C was added tetrahydroxydiboron (1.73 g, 19.39 mmol) and 4,4′-bipyridine (0.05 g, 0.32 mmol). The

resulting mixture is allowed to stir at 0°C for 15 minutes. Once the starting material was completely consumed, the reaction mixture was quenched with water and extracted thrice with ethyl acetate. The organic layer is separated, washed with brine, dried, and concentrated under reduced pressure. This was further purified by flash column chromatography to yield the pure compound TA, which was further characterized by HRMS, ^{1}H, and ^{13}C NMR techniques (2.2 g, 79% yield).

^{1}H NMR (300 MHz, DMSO-d_6): δ in ppm 7.53 (s, 1H), 7.32 (t, *J* = 7.7 Hz, 4H), 7.06 (dt, *J* = 25.0, 7.5 Hz, 8H), 6.81 (d, *J* = 8.0 Hz, 2H), 6.66 (d, *J* = 8.5 Hz, 2H), 6.54 (d, *J* = 7.9 Hz, 2H), 5.16 (s, 2H), 4.14 (q, *J* = 7.1 Hz, 2H), 1.20 (t, *J* = 7.1 Hz, 3H)

^{13}C NMR (75 MHz, DMSO-d_6): δ in ppm 168.19, 148.66, 148.36, 146.73, 138.17, 132.05, 130.97, 130.54, 130.20, 128.17, 125.61, 124.62, 123.23, 120.58, 114.41

HRMS (ESI): calc. for $[(C_{29}H_{26}N_2O_2)H]$ $(M+H)^+$ 435.2068, measured 435.2065.

Synthesis of TP:

TA (2 g, 4.6 mmol) and phthalic anhydride (750 mg, 5.06 mmol) were dissolved in 40 ml of glacial acetic acid. The mixture was refluxed under stirring for 24 hours. After the starting material was consumed, the mixture was cooled to room temperature and neutralized with a saturated sodium bicarbonate solution. The solution was extracted with ethyl acetate, washed with water and brine and the organic layer was dried over anhydrous Na_2SO_4. The pure product TP is yielded by silica gel column chromatography and characterized by HRMS, ^{1}H, and ^{13}C NMR techniques (2.1 g, 81% yield).

^{1}H NMR (300 MHz, DMSO-d_6): δ in ppm 7.97 (dd, *J* = 5.5, 3.0 Hz, 2H), 7.91 (dd, *J* = 5.5, 3.1 Hz, 2H), 7.73 (s, 1H), 7.50 (d, *J* = 8.4 Hz, 2H), 7.38 – 7.28 (m, 6H), 7.21 – 7.09 (m, 2H),

7.09 – 7.03 (m, 4H), 6.99 – 6.90 (m, 2H), 6.68 – 6.59 (m, 2H), 4.20 (d, J = 7.1 Hz, 2H), 1.23 (d, J = 7.1 Hz, 3H).

^{13}C NMR (75 MHz, DMSO-d_6): δ in ppm 167.45, 148.98, 146.49, 136.38, 135.20, 132.33, 132.04, 131.73, 130.30, 129.27, 127.92, 126.02, 125.03, 123.92, 119.89, 61.14, 14.74

HRMS (ESI): calc. for $[C_{37}H_{38}N_2O_4]$ $(M)^+$ 564.2049, measured 564.2046.

Characterisation data

^{1}H NMR of TPA-CHO:

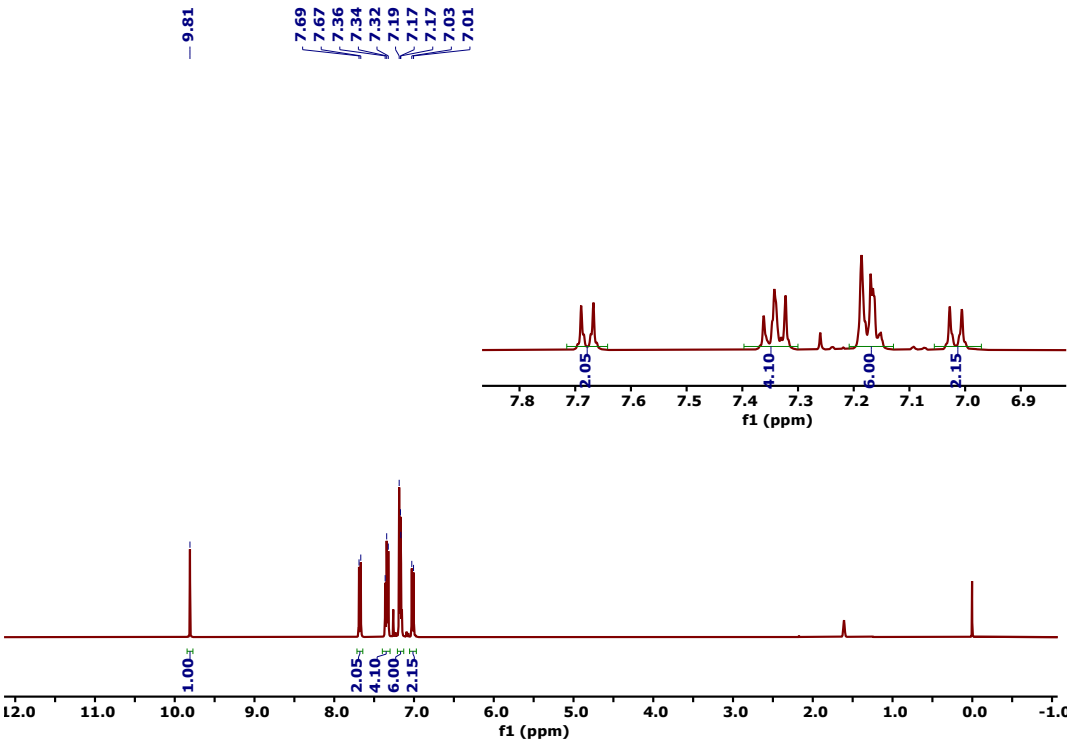

^{13}C NMR of TPA-CHO:

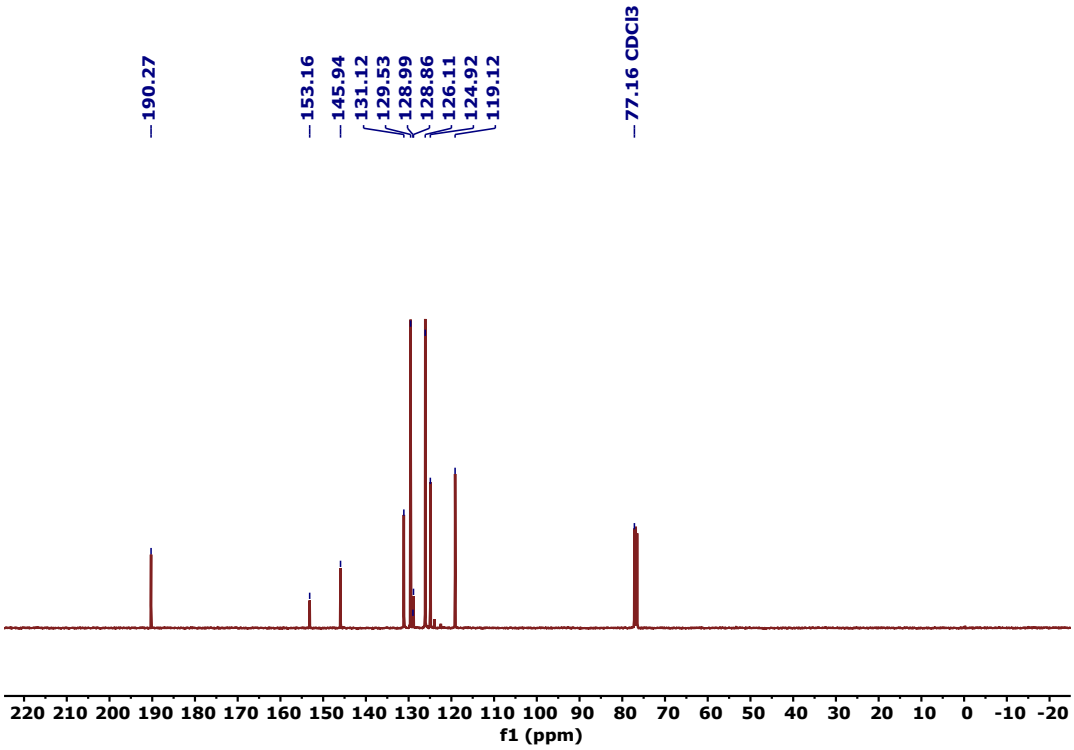

HRMS of TPA-CHO:

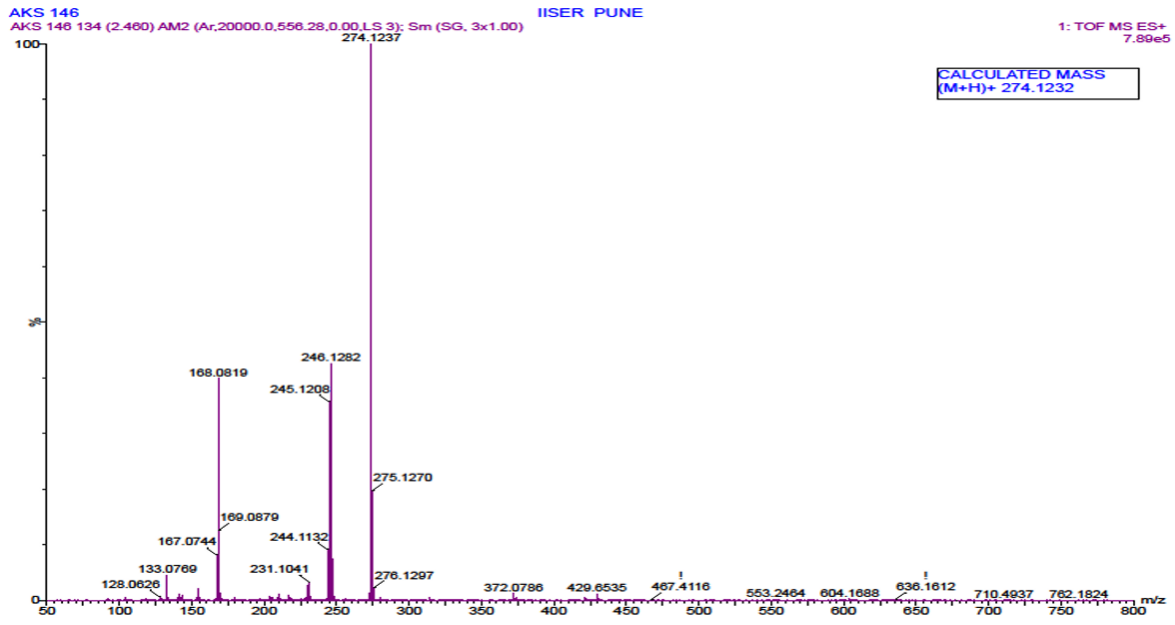

^{1}H NMR of TN:

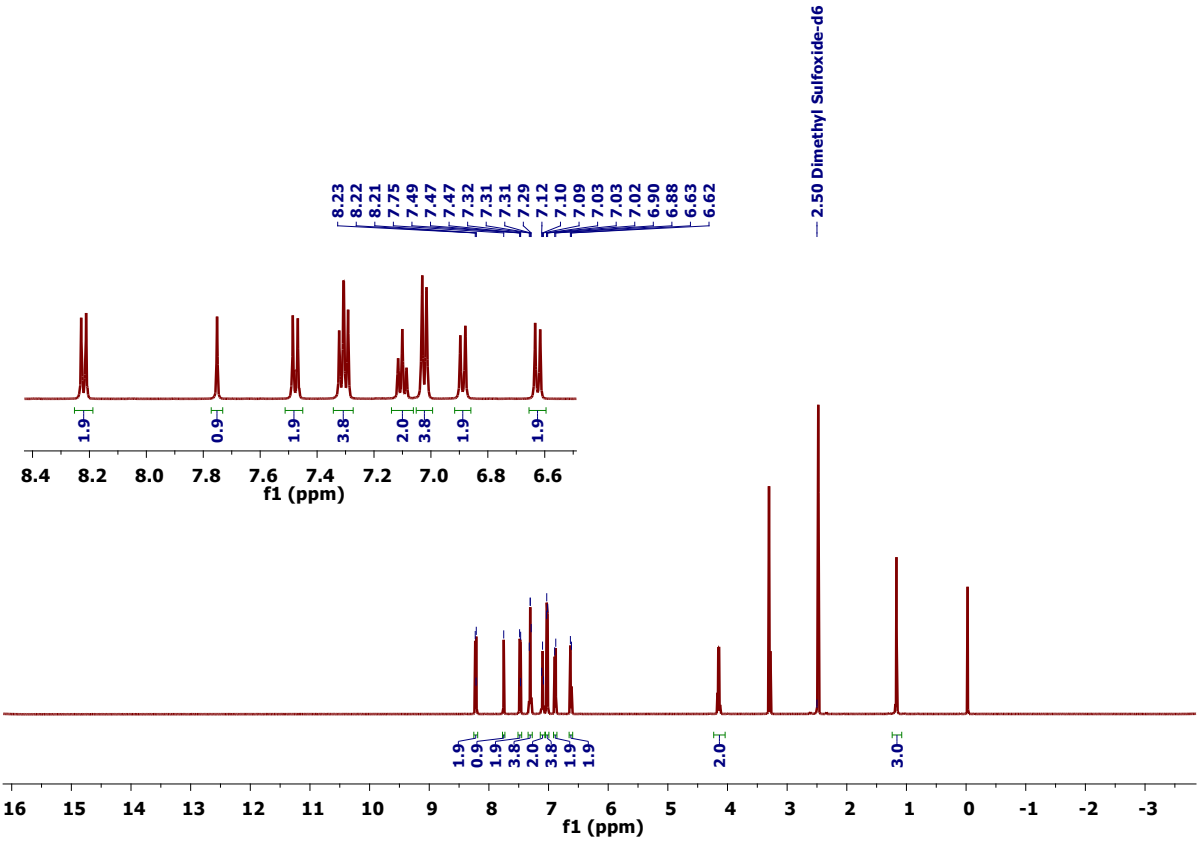

^{13}C NMR of TN:

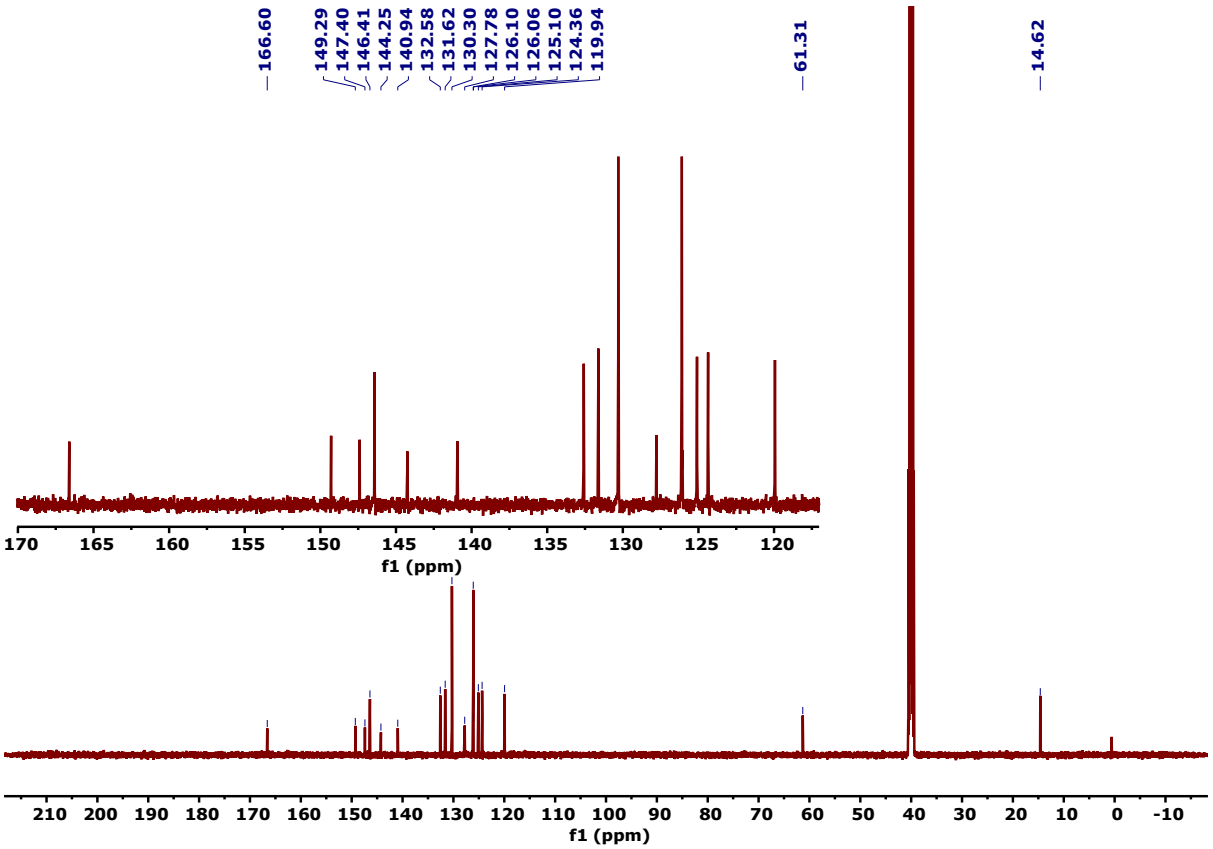

HRMS of TN:

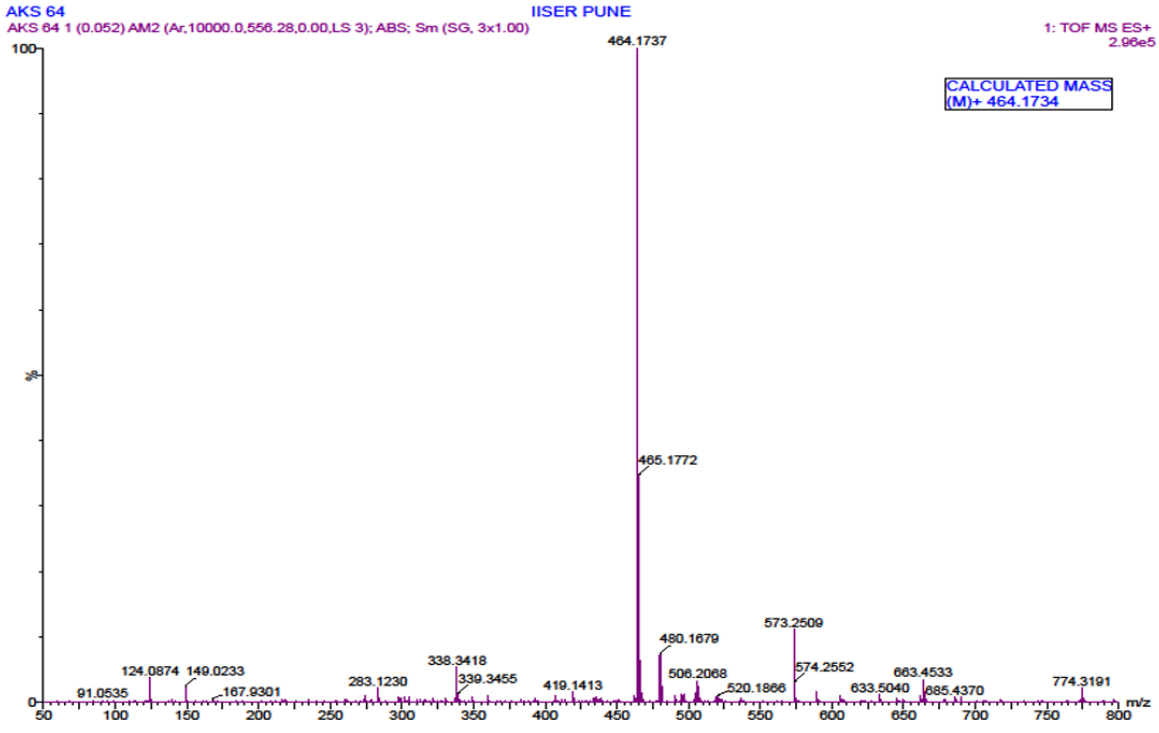

HPLC data for TN:

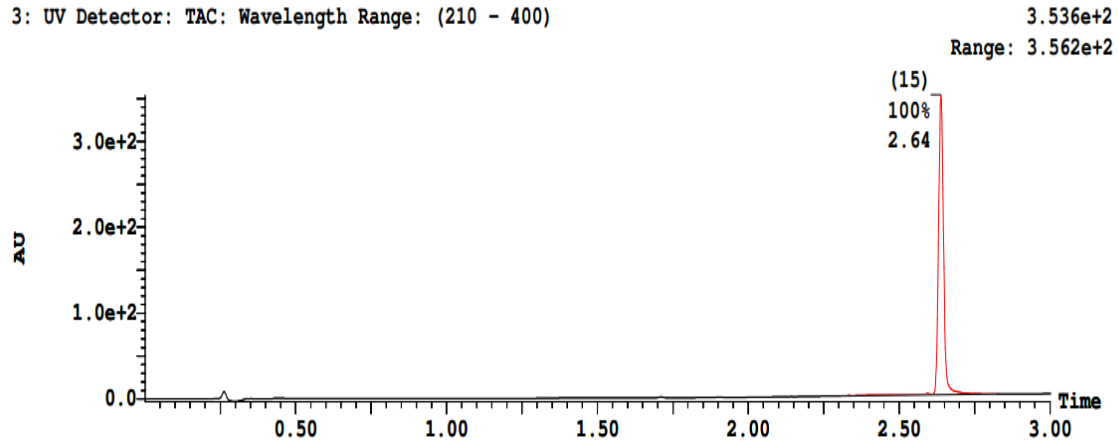

^{1}H NMR of TA:

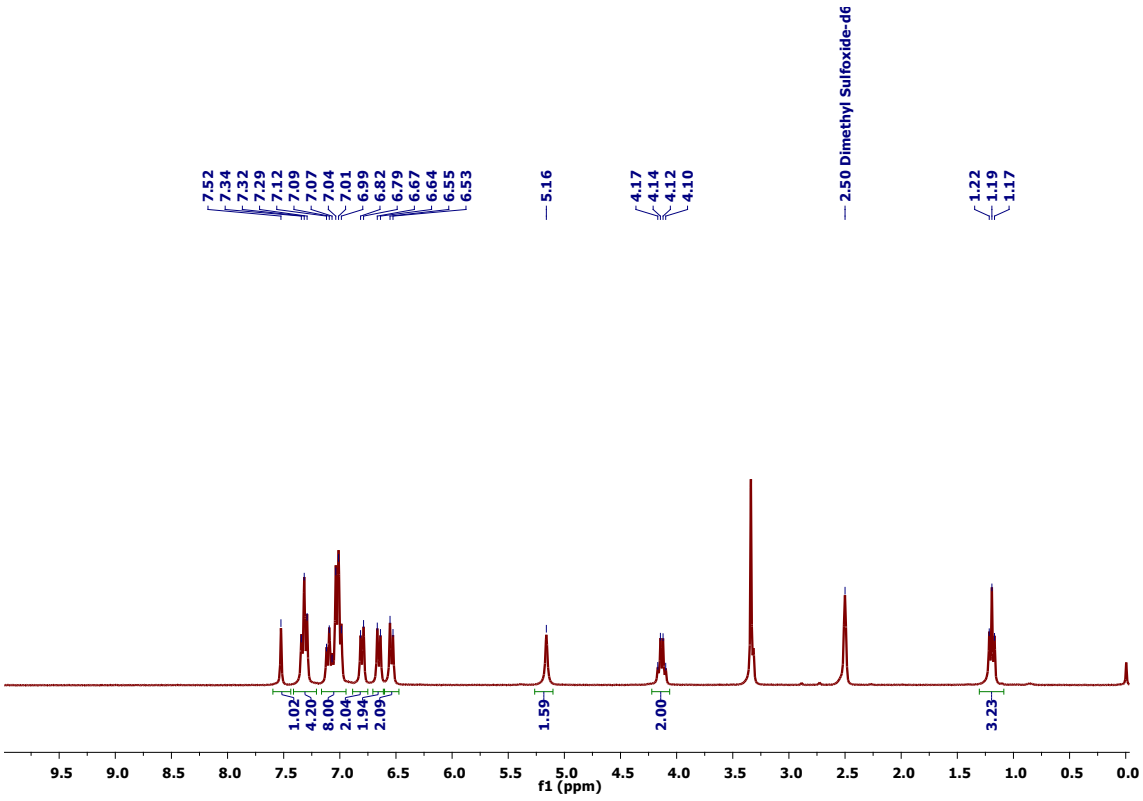

^{13}C NMR of TA:

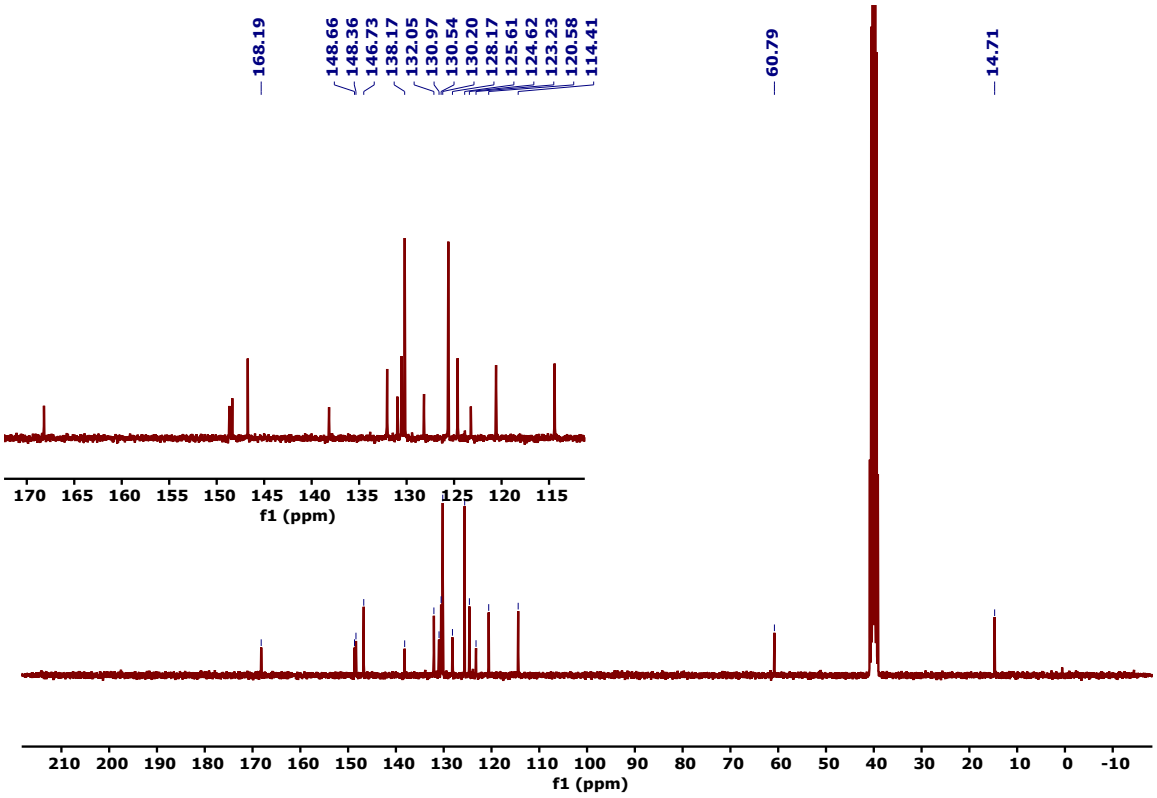

HRMS of TA:

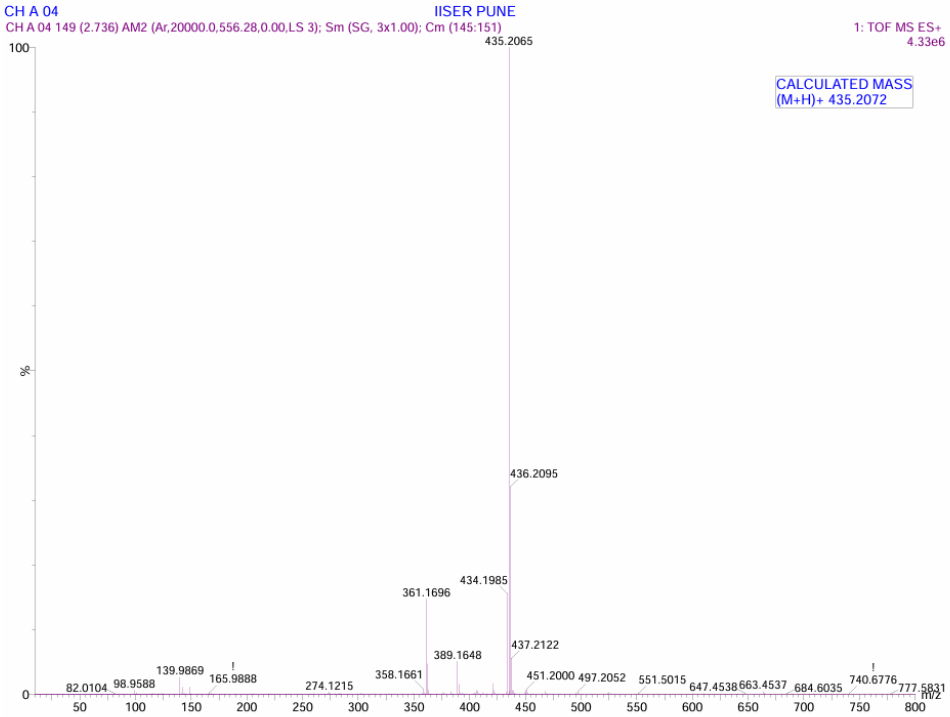

HPLC data of TA:

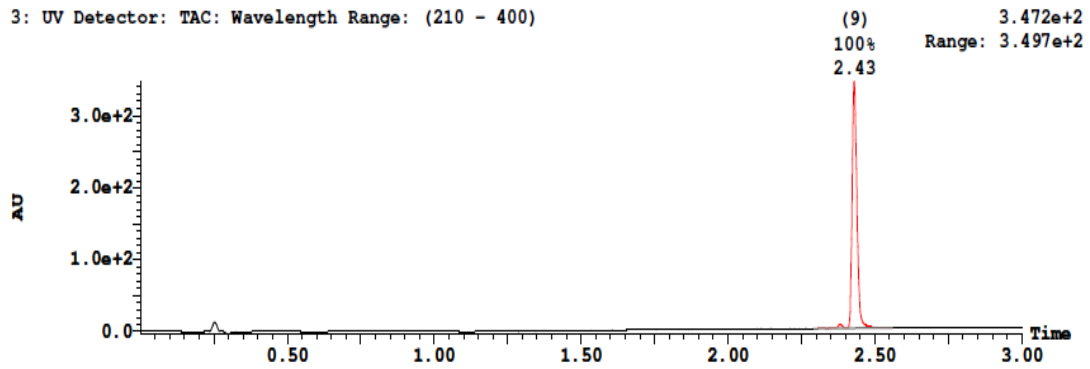

^{1}H NMR of TP:

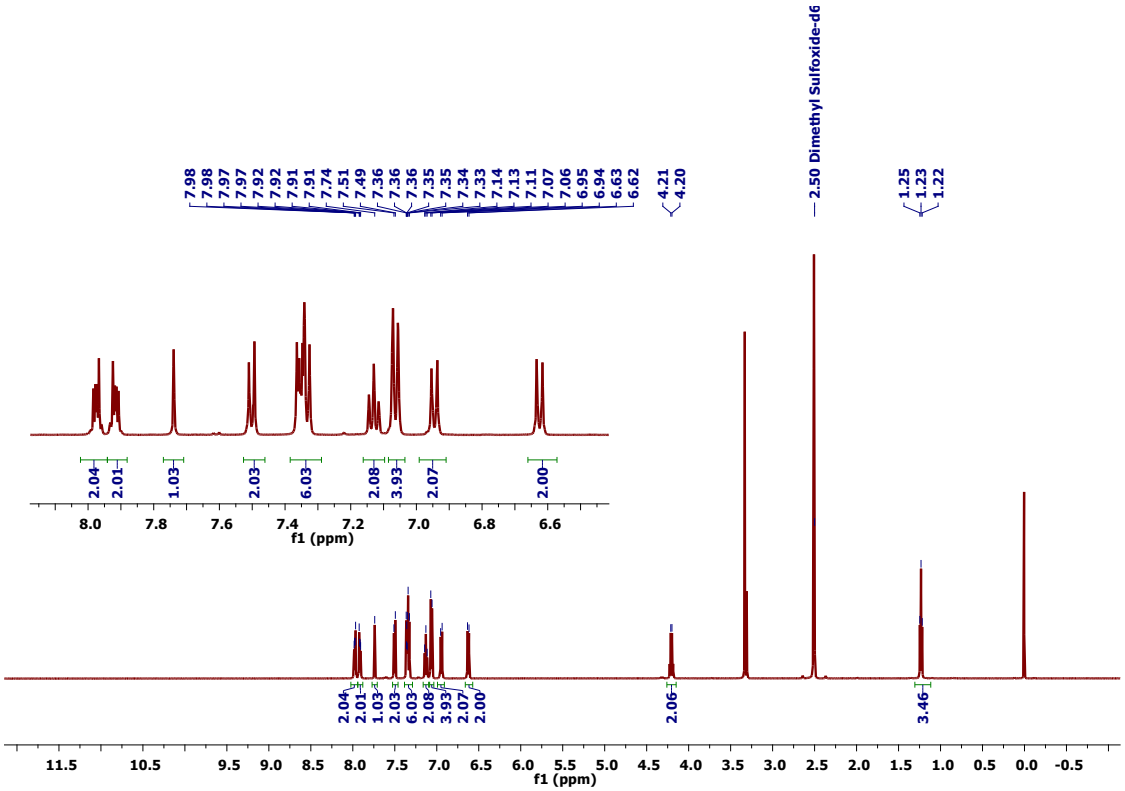

^{13}C NMR of TP:

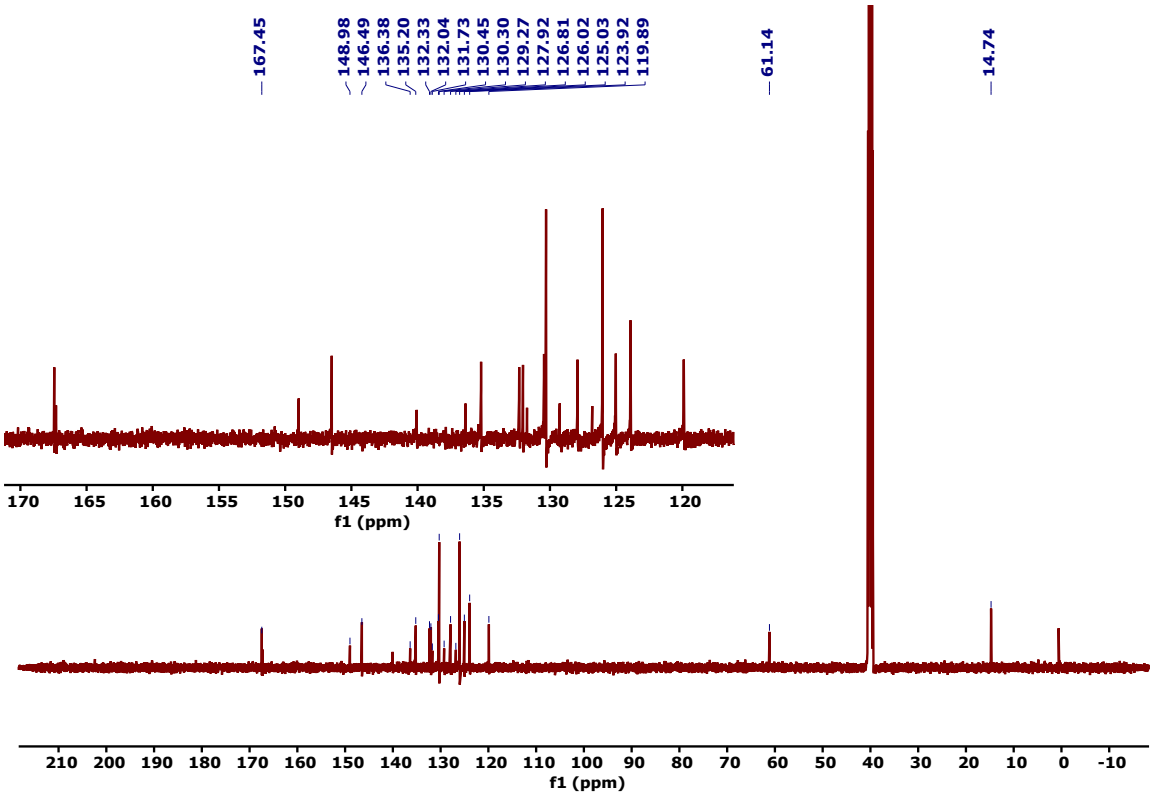

HRMS of TP:

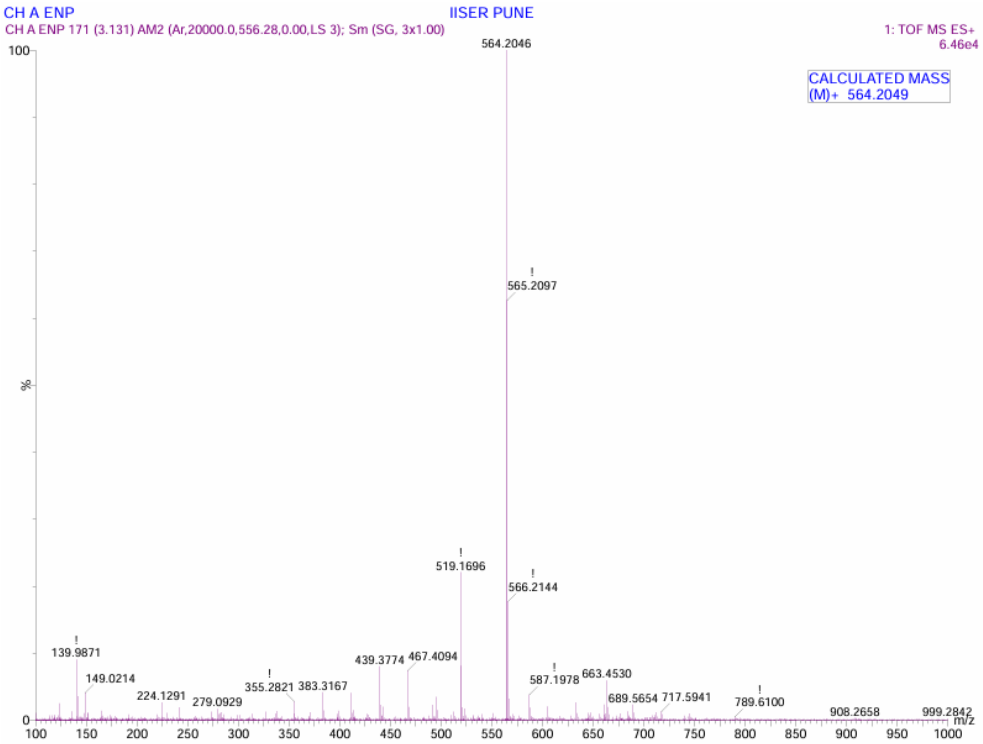

HPLC data for TP:

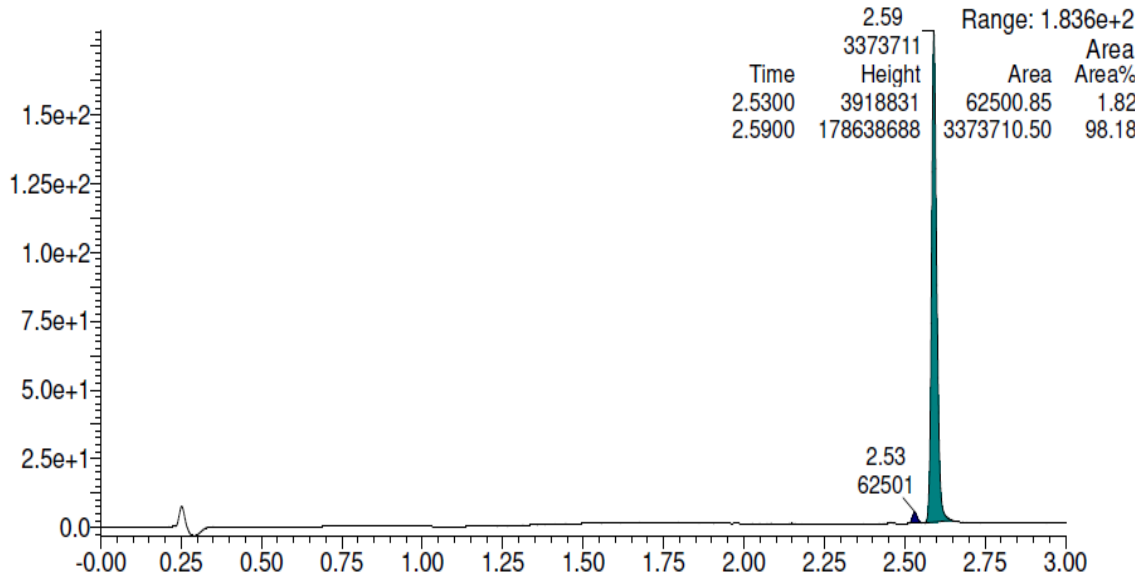

Crystallographic data

Note: All the crystals were all weakly diffracting and as a consequence data were cut at 2 theta (Θ) = 43^0 in the case of TN and TP. For TA, the data were cut at 2 theta (Θ) = 45^0. However, the data were sufficient to confirm connectivity in all cases and geometric parameters are not discussed.

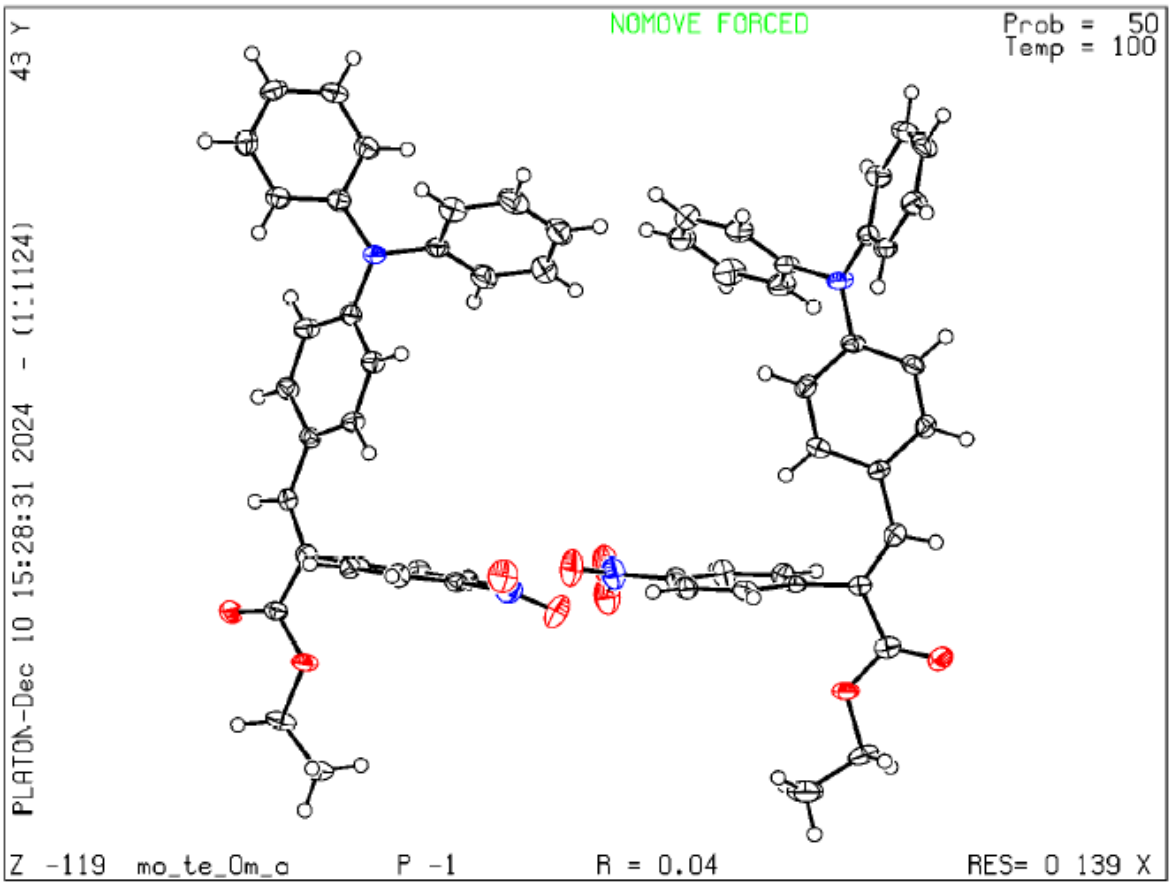

Table S1. Crystal data and structure refinement for **TN**

Identification code	TN
CCDC No.	2387501
Empirical formula	$C_{29}H_{24}N_2O_4$
Formula weight	464.50
Temperature /K	100 K
Crystal system	Triclinic
Space group	*P-1*
a/ Å	11.184(11)

b/ Å	13.742(13)
c/ Å	16.798(17)
α/°	72.17(3)
β/°	74.47(3)
γ/°	87.49(4)
Volume / Å^3	2366(4)
Z	4
ρcalc (g/cm^3)	1.304
μ/ mm^{-1}	0.088
F (0 0 0)	976
Crystal size/mm^3	0.5 × 0.03 × 0.01
Radiation	MoKα (λ = 0.71073)
2θ range for data collection/°	3.116 to 42.996
Goodness-of-fit on F^2	1.030
Final R indexes [I>=2σ (I)]	R_1 = 0.0419, wR_2 = 0.0949
Final R indexes [all data]	R_1 = 0.0660, wR_2 = 0.1102

Explanation of CheckCIF alerts for TN

Alert level A

THETM01_ALERT_3_A The value of sine(theta_max)/wavelength is less than 0.550

Calculated sin(theta_max)/wavelength = 0.5156

Explanation: This is due to the use of the OMIT command in the refinement process. Data at higher angles 2 theta (Θ) = 43^0 were omitted because I/sigma dropped below 3 indicating that the data were no longer reliable for refinement purposes. This approach was taken to ensure the accuracy and quality of the refinement process.

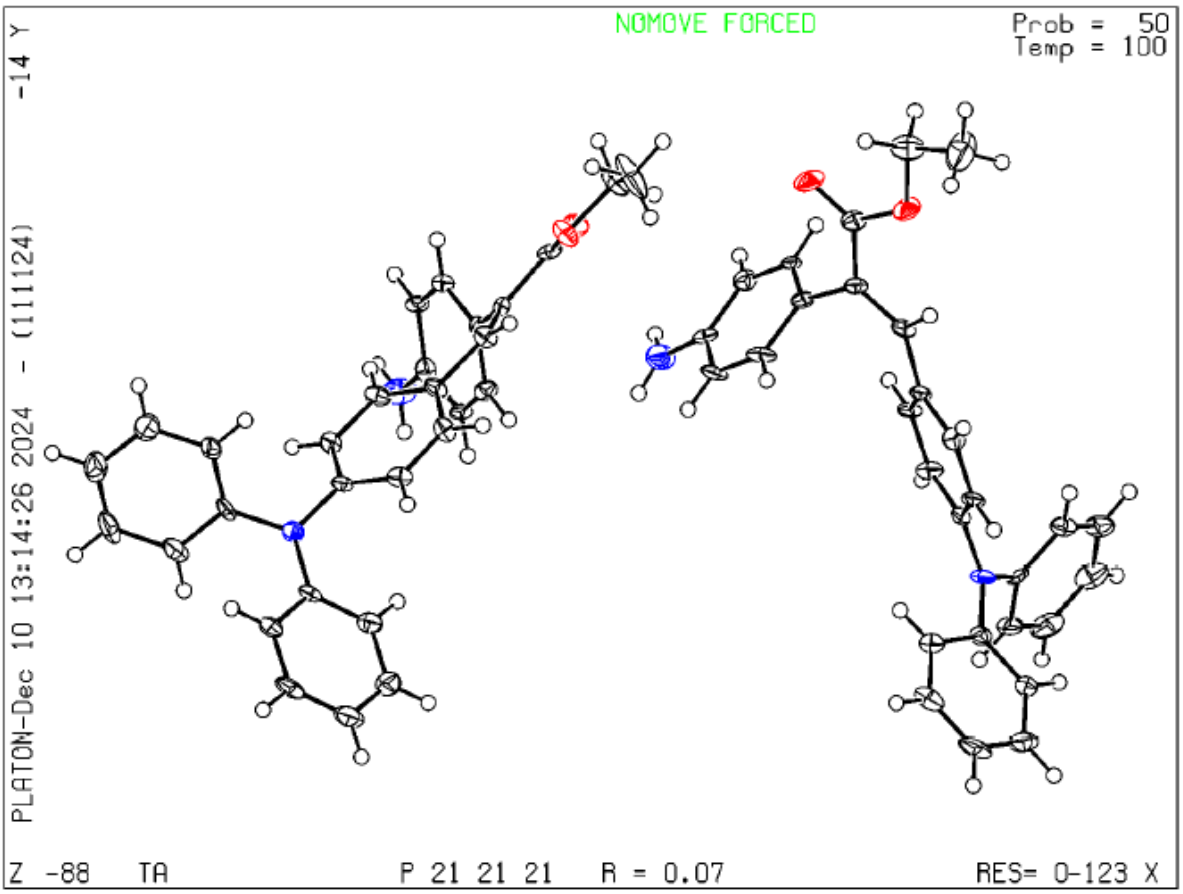

Table S2. Crystal data and structure refinement for **TA**

Identification code	TA
CCDC No.	2378737
Empirical formula	$C_{29}H_{26}N_2O_2$
Formula weight	434.52
Temperature /K	100 K
Crystal system	Orthorhombic
Space group	$P2_12_12_1$
a/ Å	11.2750(12)
b/ Å	13.8596(14)
c/ Å	29.694(3)
α/°	90
β/°	90
γ/°	90

Volume / Å^3	4640.3(8)
Z	8
ρcalc (g/cm^3)	1.244
μ/ mm^{-1}	0.078
F (0 0 0)	1840.0
Crystal size/mm^3	0.4 × 0.03 × 0.02
Radiation	MoKα (λ = 0.71073)
2θ range for data collection/^{o}	3.864 to 44.992
Goodness-of-fit on F^2	1.076
Final R indexes [I>=2σ (I)]	R_1 = 0.0661, wR_2 = 0.1381
Final R indexes [all data]	R_1 = 0.1017, wR_2 = 0.1539

Explanation of CheckCIF alerts for TA

Alert level A

THETM01_ALERT_3_A The value of sine(theta_max)/wavelength is less than 0.550 Calculated sin(theta_max)/wavelength = 0.5383

Explanation: This is due to the use of the OMIT command in the refinement process. Data at higher angles 2 theta (Θ) = 45^0 were omitted because I/sigma dropped below 3 indicating that the data were no longer reliable for refinement purposes. This approach was taken to ensure the accuracy and quality of the refinement process.

Alert level B

RINTA01_ALERT_3_B The value of Rint is greater than 0.18 Rint given 0.244

Explanation: The high R_{int} arises from weak diffraction due to the poor quality of the crystal Efforts to obtain better crystals were unsuccessful.

PLAT340_ALERT_3_B Low Bond Precision on C-C Bonds ..... 0.01147 Å.

Explanation: It is due to poor quality data of weakly diffracted crystals.

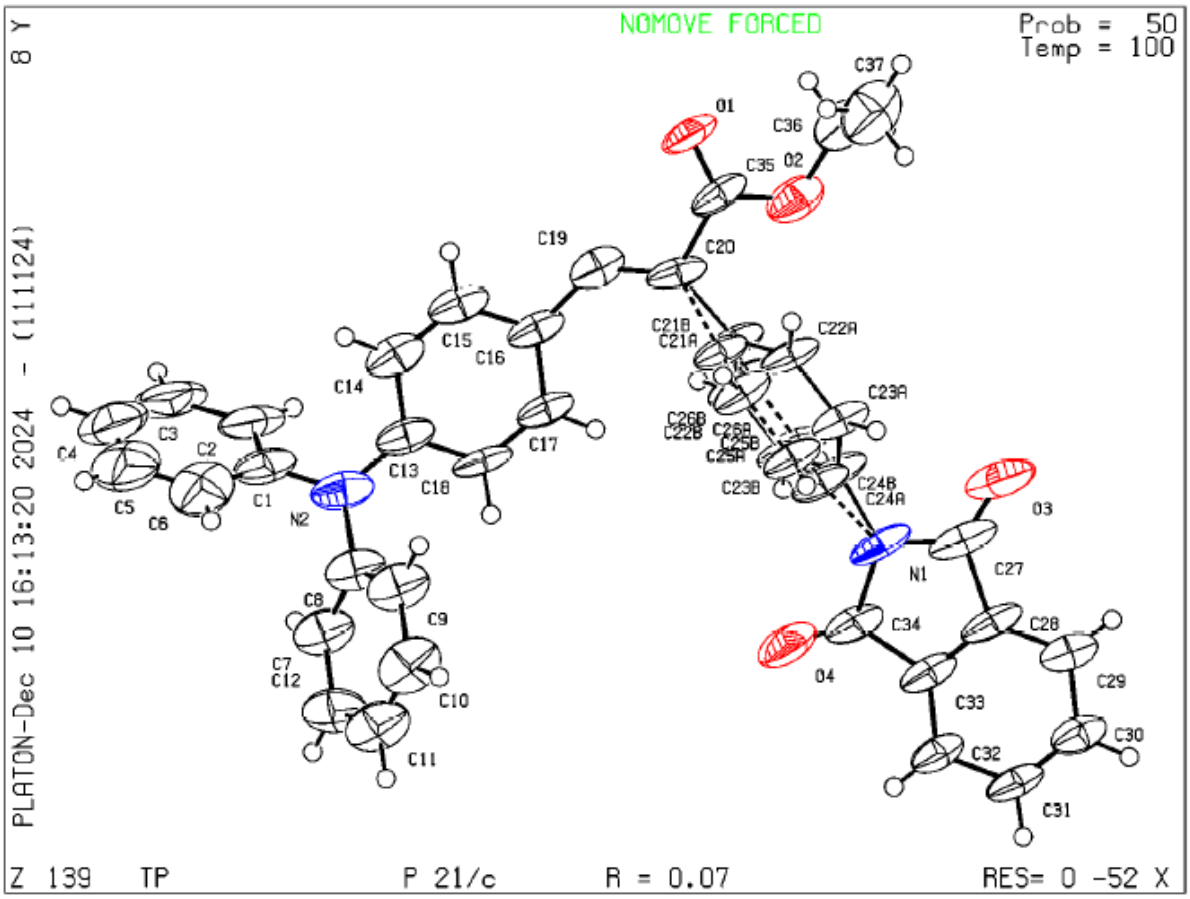

Table S3. Crystal data and structure refinement for **TP**

Identification code	TP
CCDC No.	2387502
Empirical formula	$C_{37}H_{27}N_2O_4$
Formula weight	563.60
Temperature /K	100 K
Crystal system	Monoclinic
Space group	*P2₁/c*
a/ Å	15.833(7)
b/ Å	10.282(4)
c/ Å	18.493(7)
α/°	90
β/°	103.027(11)
γ/°	90

Volume / Å^3	2933(2)
Z	4
ρcalc (g/cm^3)	1.276
μ/ mm^{-1}	0.083
F (0 0 0)	1180.0
Crystal size/mm^3	0.4 × 0.2 × 0.05
Radiation	MoKα (λ = 0.71073)
2θ range for data collection/^{o}	4.522 to 42.996
Goodness-of-fit on F^2	1.012
Final R indexes [I>=2σ (I)]	R_1 = 0.0699, wR_2 = 0.1458
Final R indexes [all data]	R_1 = 0.1638, wR_2 = 0.2053

Explanation of CheckCIF alerts for TP

Alert level A

THETM01_ALERT_3_A The value of sine(theta_max)/wavelength is less than 0.550 Calculated sin(theta_max)/wavelength = 0.5156

Explanation: This is due to the use of the OMIT command in the refinement process. Data at higher angles 2 theta (Θ) = 43^0 were omitted because I/sigma dropped below 3 indicating that the data were no longer reliable for refinement purposes. This approach was taken to ensure the accuracy and quality of the refinement process.

Alert level B

PLAT340_ALERT_3_B Low Bond Precision on C-C Bonds ..... 0.014 Å.

Explanation: This is due to poor quality data of weakly diffracted crystals.

Photophysical and theoretical studies

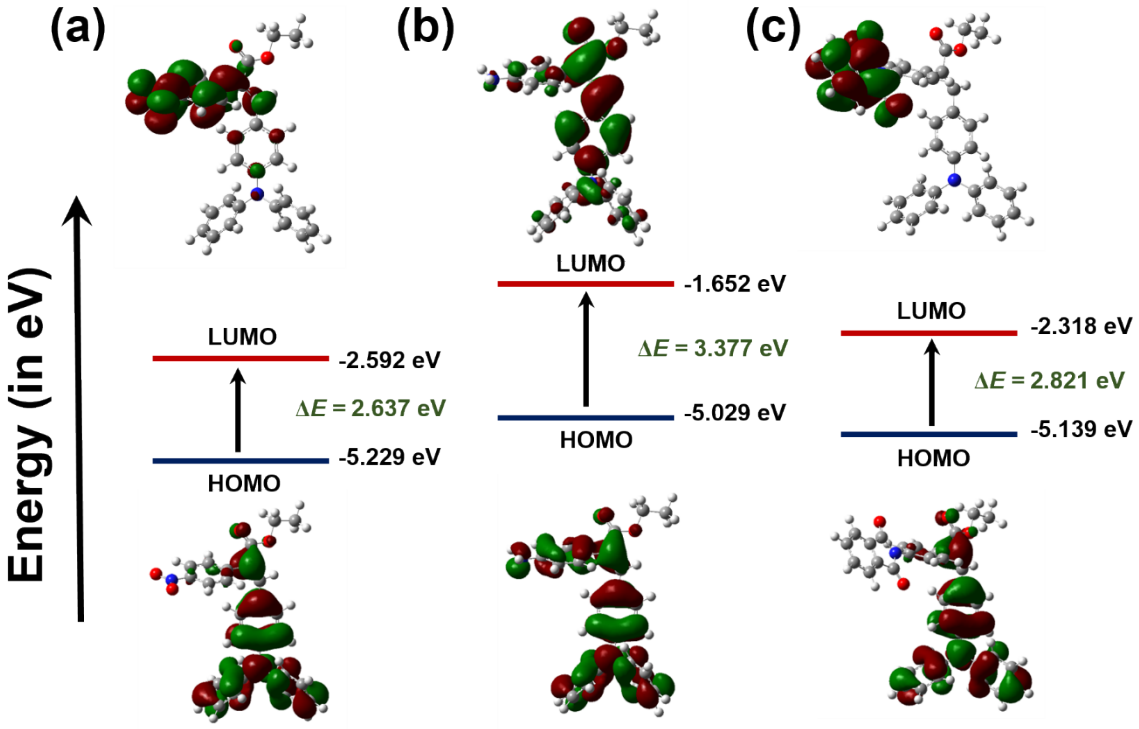

Figure S1. HOMO and LUMO molecular orbitals in the ground state optimized structures of (a) TN, (b) TA, and (c) TP.

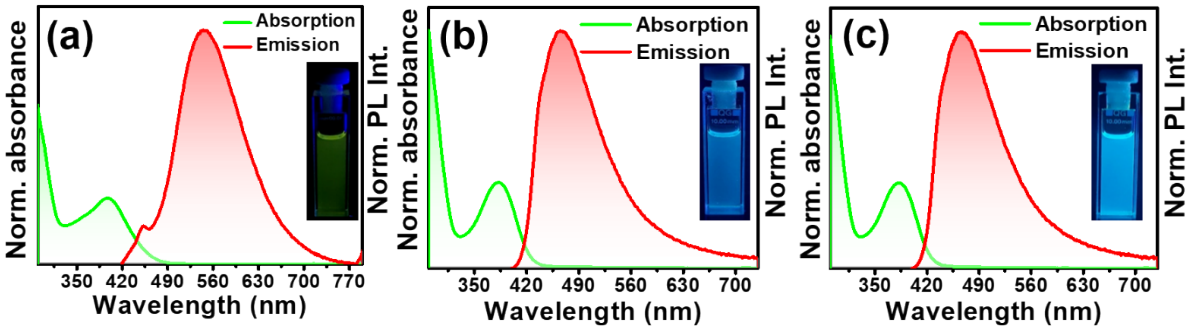

Figure S2. Absorption and emission spectra in toluene of (a) TN, (b) TA and, (c) TP. Inset: Cuvette images of the toluene solutions under UV irradiation. (Concentration: 30 μM)

Excited State	Energy (eV)	Wavelength (nm)	Orbital configuration	Oscillator strength (*f*)
1 (T_1)	2.0159	615	HOMO-1 to LUMO HOMO-1 to LUMO+1 HOMO to LUMO HOMO to LUMO+1	0.000

2 (S_1)	2.2548	550	HOMO to LUMO	0.135
6 (S_2)	3.0530	406	HOMO to LUMO+1	0.750

Table S4. Excited state parameters of TN at Franck-Condon geometry of the ground state.

Excited State	Energy (eV)	Wavelength (nm)	Orbital configuration	Oscillator strength (*f*)
1 (T_1)	2.1573	575	HOMO-2 to LUMO HOMO to LUMO	0.000
2 (S_1)	2.9259	424	HOMO-1 to LUMO HOMO to LUMO	0.702
5 (S_2)	3.3090	375	HOMO-1 to LUMO HOMO to LUMO	0.160

Table S5. Excited state parameters of TA at Franck-Condon geometry of the ground state.

Excited State	Energy (eV)	Wavelength (nm)	Orbital configuration	Oscillator strength (*f*)
1 (T_1)	2.193	565	HOMO-2 to LUMO+1 HOMO-1 to LUMO+1 HOMO to LUMO+1	0.000
2 (T_2)	2.5015	496	HOMO to LUMO	0.000
3 (S_1)	2.5090	494	HOMO to LUMO	0.000
4 (S_2)	2.9770	417	HOMO to LUMO+1	0.815

Table S6. Excited state parameters of TP at Franck-Condon geometry of the ground state.

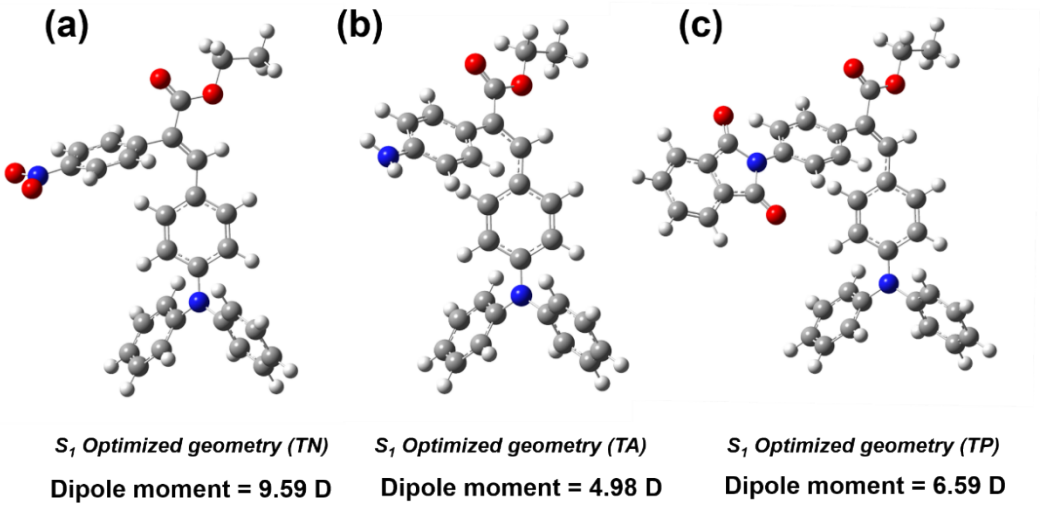

Figure S3. Optimized S_1 molecular geometries of (a) TN, (b) TA, and (c) TP. For S_1 state optimization, the TD-SCF method and B3LYP/6-31G (d, p) level of theory have been used in THF solvent using the IEFPCM solvent model. The dipole moments in the S_1 excited state are found to be 9.59 D, 4.98 D, and 6.59 D for TN, TA, and TP, respectively.

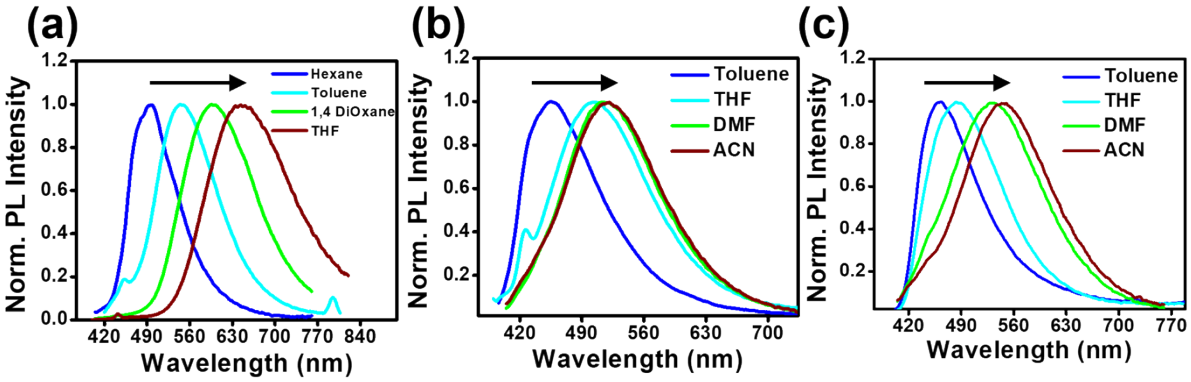

Figure S4. Solvatochromic emission studies of all three luminogens- (a) TN, (b) TA, and (c) TP in solvents of different polarities.

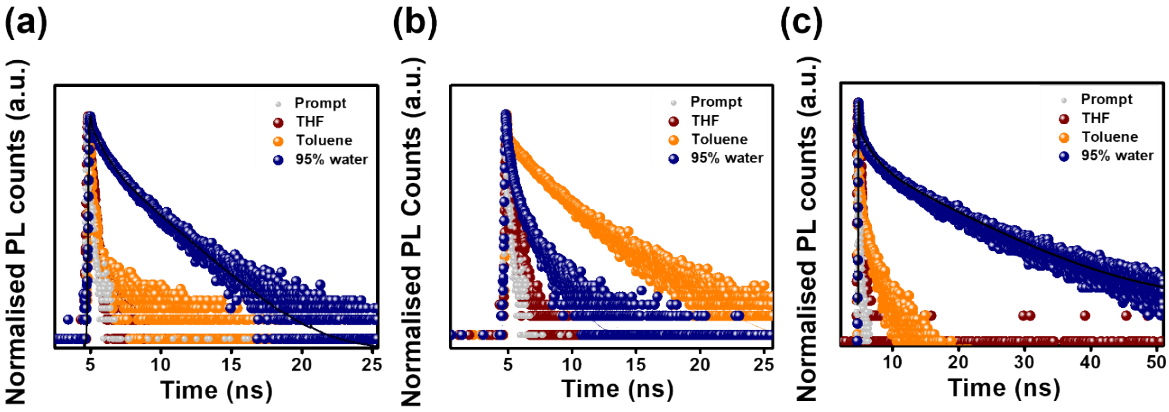

Figure S5. Time-resolved fluorescence decay profiles of (a) TN, (b) TA, and (c) TP in the nanosecond time scale (λ_{ex} = 375 nm). Solutions are made with a concentration of 20 μM. (Note: Decays with τ_{av} < 50 ps fall below the detection limit of the TCSPC instrument and hence have not been fitted).

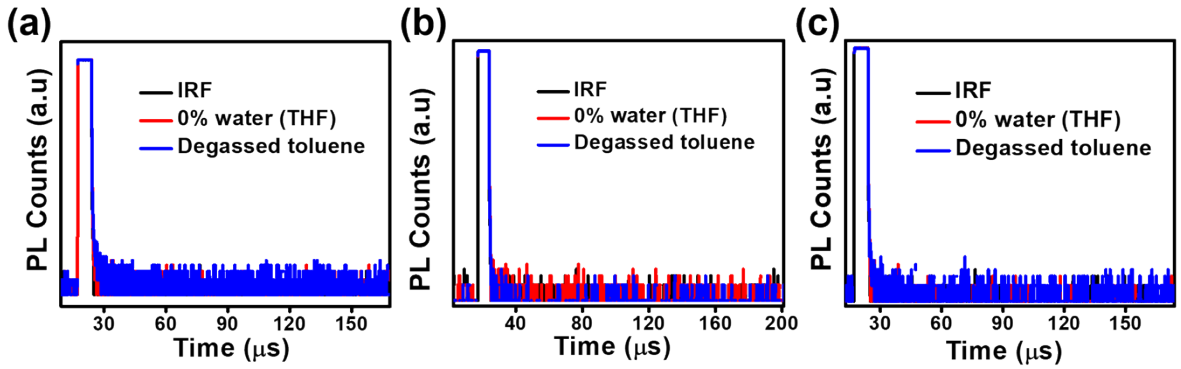

Figure S6. Time-resolved fluorescence decay profiles of (a) TN, (b) TA, and (c) TP in the micro-second time scale (λ_{ex} = 357 nm). No lifetime component in ~μs-ms region found in all three. Solutions are made with a concentration of 20 μM.

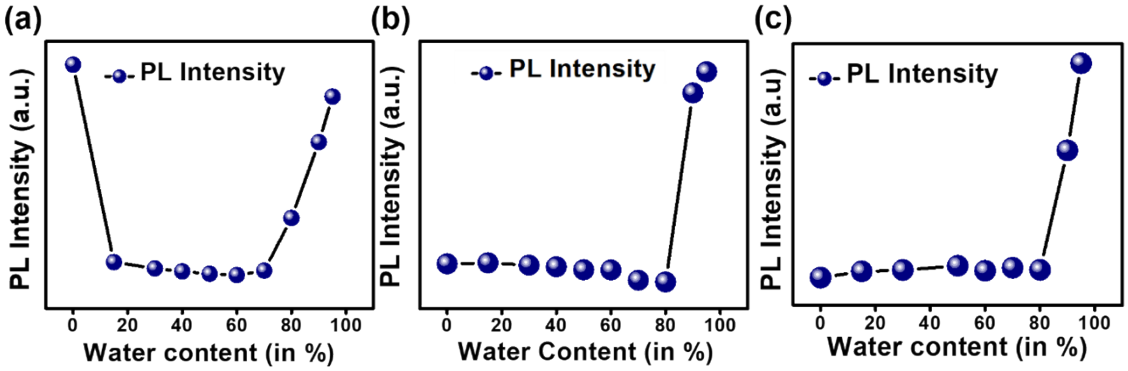

Figure S7. Photoluminescence intensity of THF-water binary solutions of (a) TN, (b) TA, and (c) TP plotted against the water content.

Water content (in %)	PLQY (TN)	PLQY (TA)	PLQY (TP)
0%	***9.9%***	***2.7%***	***4.9%***
15%	0.8%	2.8%	6%
30%	0.6%	2.7%	6.3%
50%	0.5%	2.5%	7%
60%	0.5%	2.5%	6.1%
70%	0.8%	2%	6.7%
80%	3%	2%	6.3%
90%	6%	10.1%	27.8%
95%	***7%***	***13%***	***45%***

Table S7. PLQY variation of all three luminogens in different water content.

Note 1: Explanation of AIE from crystal packing and intermolecular non-covalent interaction analysis

The aggregation-induced emission (AIE) characteristics of the luminogens can be linked to their crystal packing, specifically due to the suppression of detrimental π···π stacking interactions in the aggregated state. Stronger π···π interactions can increase planarity and exciton−phonon coupling in the solid state, often leading to reduced emission. Effective π···π stacking interactions typically occur within a distance of 3.3-3.8 Å;[9] beyond this range, their strength diminishes, making aggregation-caused quenching (ACQ) less likely. For the three luminogens under investigation, an analysis of their crystal structures reveals increased distances for potential π···π stacking interactions: 6.1 Å for TN, 4.7 Å for TA, and 5.1 Å for TP (Fig. S8a, d, g). Additionally, the space-filling model demonstrates that the planar aromatic groups of neighboring molecules are positioned in a manner that prevents significant π···π

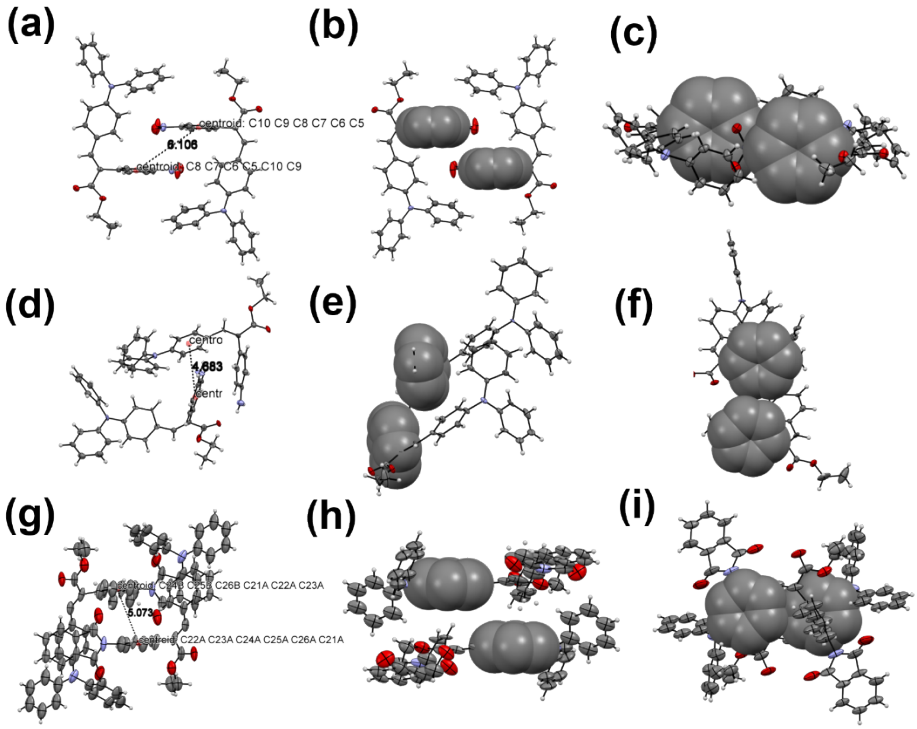

Figure S8. π···π stacking interactions distance of two neighboring molecules of (a) TN, (b) TA and (c) TP. Spacefilling model of (b) TN, (e) TA and (h) TP from side-view. Spacefilling model of (c) TN, (f) TA and (i) TP from top-view.

overlap, further reducing the likelihood of quenching (Fig. S8b, e, h, c, f, i).

Here, the best possible way to depict the intermolecular interaction is the Hirshfeld surface analysis. The concept of Hirshfeld surface originated from an attempt to give an idea of space occupied by a molecule in a crystal for the purpose of partitioning the crystal electron density into molecular fragments.[10-12] d_e and d_i are the two interactions to be mapped on the Hirshfeld surface; where d_e is the distance of an atom external to the generated Hirshfeld surface and d_i is the distance of an atom internal to the Hirshfeld surface. These two values together generate a 2-D fingerprint plot where different colors indicate the frequency of occurrence of interaction. In this regard, the normalized contact distance based on d_e, d_i, and the van der Waals radii of the atom enables the identification of the region of importance to intermolecular interactions.[10-12] The d_{norm} values are mapped onto the Hirshfeld surface by a red-white-blue color scheme, where the red color indicates closer contact and negative d_{norm} value, the blue region suggests

longer contact and positive d_{norm} value, and the white color indicates the distance of contact exactly equal to the van der Waals separation and a d_{norm} value equals to zero.[10-13] Here in this work, the Hirshfeld surface of all the designed luminogens is generated using Crystal Explorer 3.1 software with an iso-value of 0.5.[13]

In all three crystals, the 2-D fingerprint plot reveals minimal π···π stacking interactions, accounting for less than 5% and characterized by weak strength (shown in blue) (Fig. S9). This finding supports the AIE properties of the molecules. Furthermore, we evaluated the strength and impact of other short intermolecular contacts that create a constrained environment, limiting the motion of high-energy bond vibrations (with C−H stretching around 0.37 eV in aromatic compounds).[14] This restriction helps to decrease nonradiative deactivation in the aggregated or solid state, thus enhancing the AIE effect. Notably, significant contributions from C−H···π interactions (approximately 10.3 kJ/mol)[15] and C−H···O interactions (typically between 41−104 kJ/mol)[16] were identified, with the latter exhibiting strong interactions (indicated by red patches) (Fig. S9), which further promote the AIE characteristics.

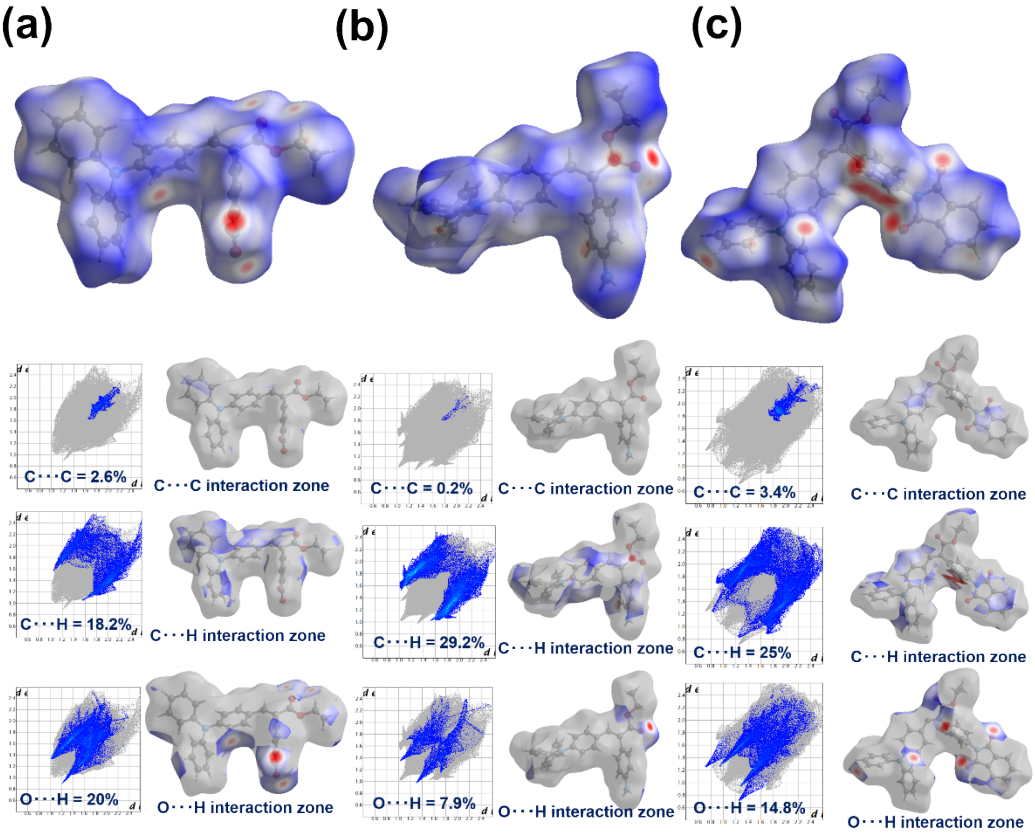

Figure S9. Normalized distance (d_{norm}) mapped over Hirshfeld surface of each luminogen ((a) TN, (b) TA and (c) TP) along with generated finger print plots obtained from d_{norm} to decipher percentage of each type of non-covalent interaction. The grey part in the finger print plot indicates total interactions.

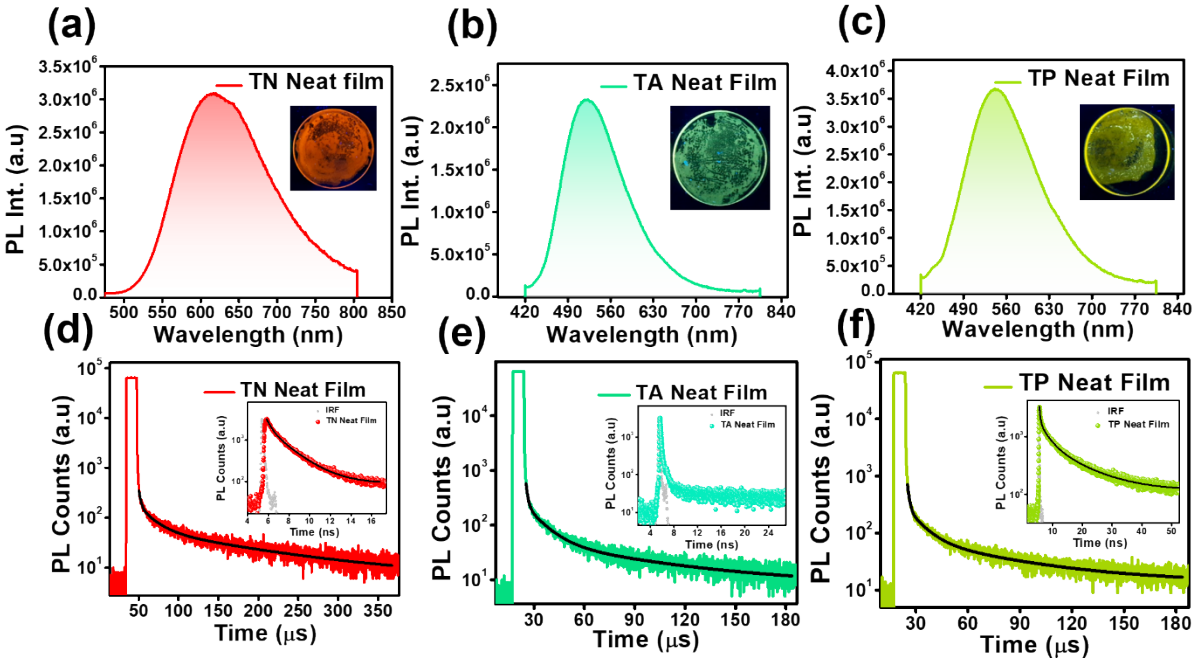

Figure S10. Steady-state emission spectra for the neat film of (a) TN, (b) TA, and (c) TP (inset shows the UV excited neat film emission) and time-resolved emission decay profiles (λ_{ex} = 357 nm) for the neat film of (d) TN, (e) TA, and (f) TP in the microsecond time scale (λ_{ex} = 357 nm) (inset shows the decay profiles in the nanosecond time scale, λ_{ex} = 375 nm). The average delayed fluorescence lifetime (τ_{DF}) of TN, TA, and TP neat films were found to be 27.3 μs, 8.64 μs, and 7.83 μs respectively. (Note: Decays in the nanosecond time scale with τ_{av} < 50 ps fall below the detection limit of the TCSPC instrument and hence have not been fitted).

Note 2: Role of any trapped solvent residue in neat film emission

To demonstrate that residual solvent molecules do not influence the emission in the neat films or solvatochromic emission of solvents does not play any role in it, we compared the emissions of films made from solvents of different polarities, specifically THF (polarity index 4.0) and acetonitrile (polarity index 5.8). We found no significant changes in emission features among all three luminogens (Fig. S11), indicating that trapped solvent molecules do not play a role in the emission process.

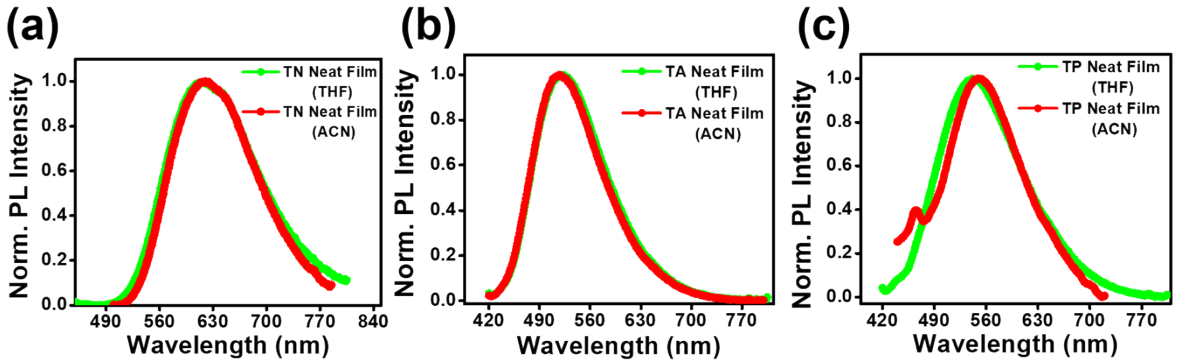

Figure S11. Steady-state emissions of neat films for (a) TN, (b) TA, and (c) TP were made from solvents of different polarities, i.e., THF and acetonitrile.

Additionally, we recorded and compared PL excitation spectra for the solution phase (monomeric state) and neat films. The significant differences in spectral onset and width between the two phases suggest that aggregation occurs in the neat films (Fig. S12), which induces exciton coupling and alters the spectral features. Thus, the observed change in emissions from neat films results from the alteration of excited state energy levels due to aggregation, rather than from trapped solvent residue.

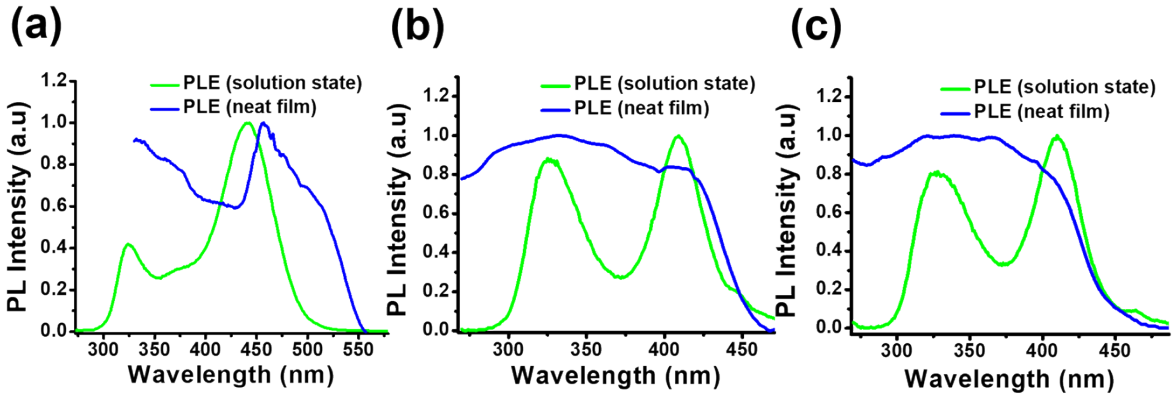

Figure S12. PL excitation spectra of solution phase (THF as solvent) and neat films of (a) TN, (b) TA, and (c) TP.

Note 3: Crystalline/amorphous nature of the neat films

Figure S13. PXRD patterns of the crystals of (a) TN, (b) TA, and (c) TP. PXRD patterns of the neat films of (d) TN, (e) TA, and (f) TP.

A PXRD (Powder X-ray Diffraction) experiment was conducted to determine the crystalline or amorphous nature of the neat films. The PXRD patterns for both TN and TA exhibited no sharp or intense diffraction peaks, but instead displayed a broad halo, indicating that the neat films of TN and TA are amorphous (Fig. S13). In contrast, the PXRD pattern for TP showed several sharp and intense diffraction peaks, suggesting that the TP neat films possess a higher level of crystallinity (Fig. S13). The crystals of all three luminogens show distinct and intense

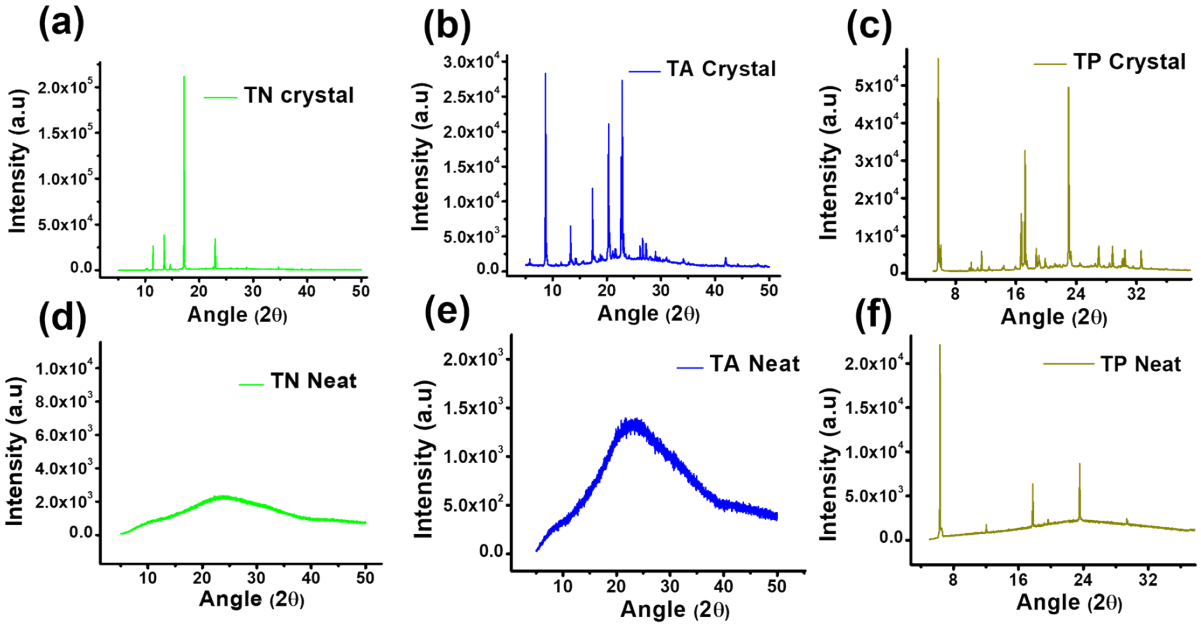

diffraction peaks in their PXRD patterns (although PXRD patterns of crystals always lead to selective diffraction from some planes due to their mostly single crystalline nature). In contrast, the films of TN and TA are amorphous, meaning they do not maintain the same arrangement as observed in the crystals. However, for TP, the diffraction peaks obtained from the neat film closely match the positions seen in the crystals, indicating that it retains a similar structural arrangement (Fig. S13).

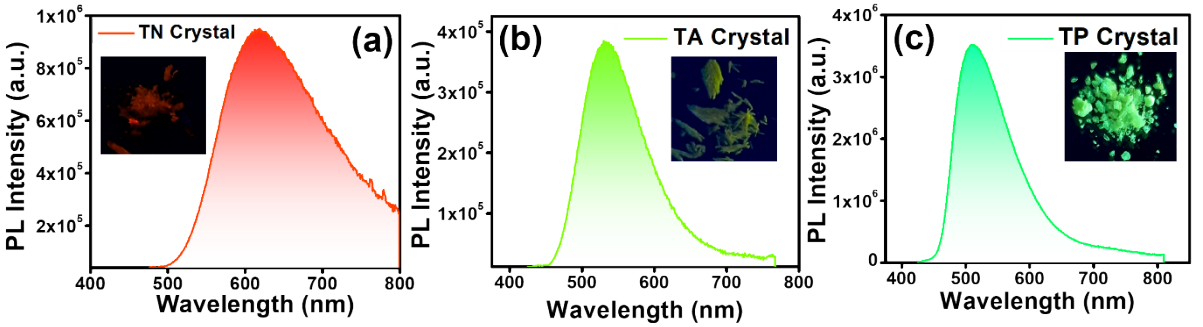

Figure S14. Steady-state emission spectra of the crystals of (a) TN, (b) TA, and (c) TP along with the UV (365 nm) excited crystal emission shown in the insets.

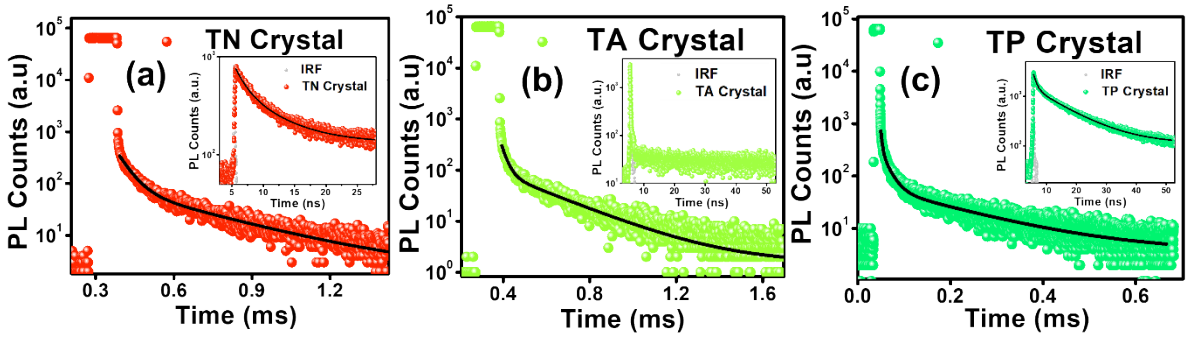

Figure S15. Time-resolved emission decay profiles for the crystals of (a) TN, (b) TA, and (c) TP in the sub-millisecond time scale (λ_{ex} = 357 nm). Insets show the decay profiles in the nanosecond time scale (λ_{ex} = 375 nm). Average delayed fluorescence lifetime (τ_{DF}) of TN, TA, and TP crystals were found to be 104 µs, 86 µs, and 20 µs respectively. (Note: Decays in the nanosecond time scale with τ_{av} < 50 ps fall below the detection limit of the TCSPC instrument and hence have not been fitted).

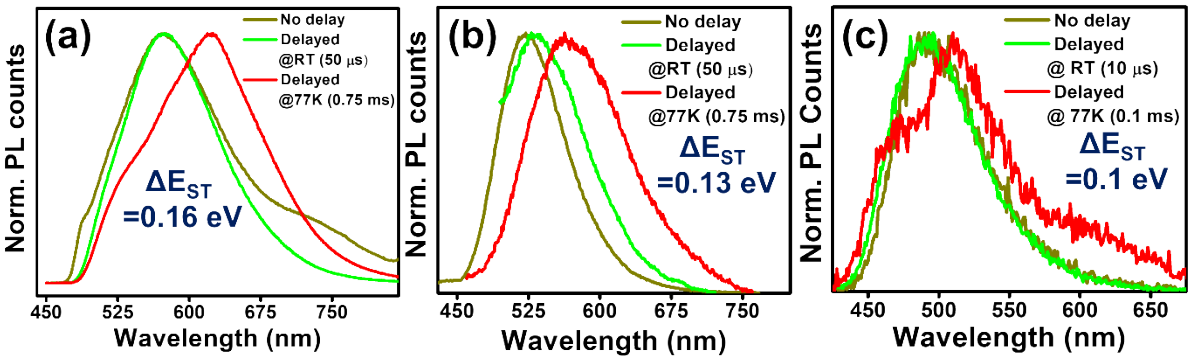

Figure S16. Time-gated emission spectra for the crystals of (a) TN, (b) TA, and (c) TP at RT (298 K) and 77 K with different delays. Experimentally calculated ΔE_{ST} is obtained from the emission peak positions. Time delays of detection for all spectra are mentioned. For the collection of delayed spectra at RT, a 5 ms sample window has been employed for TN and TA and a 500 µs sample window for TP. The sample window for emission measurements at 77 K is kept at 10 ms for all three crystals.

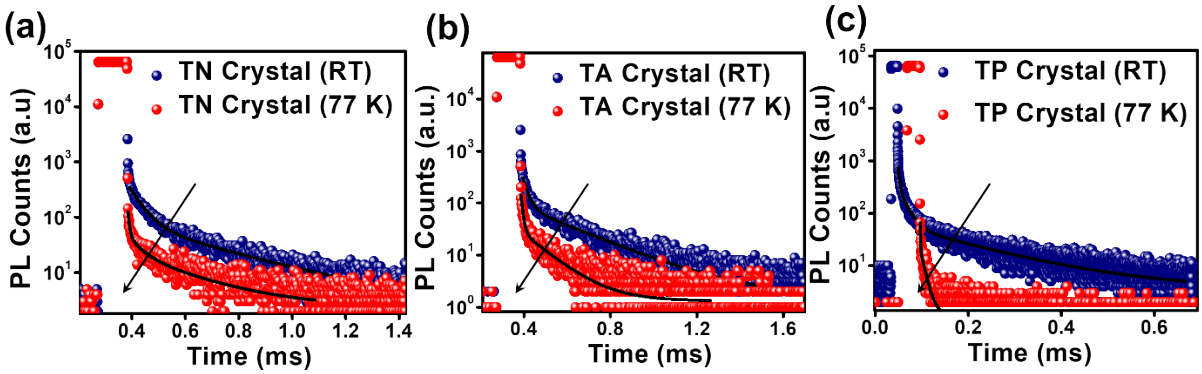

Figure S17. Time-resolved emission decay profiles (λ_{exc} = 357 nm) for the crystals of (a) TN, (b) TA, and (c) TP at RT (298 K) and 77 K. Average delayed fluorescence lifetime (τ_{DF}) of TN, TA and TP crystals at RT were found to be 104 µs, 86 µs and 20 µs respectively and at 77 K, their lifetimes were reduced to 48 µs, 31 µs and 3 µs respectively.

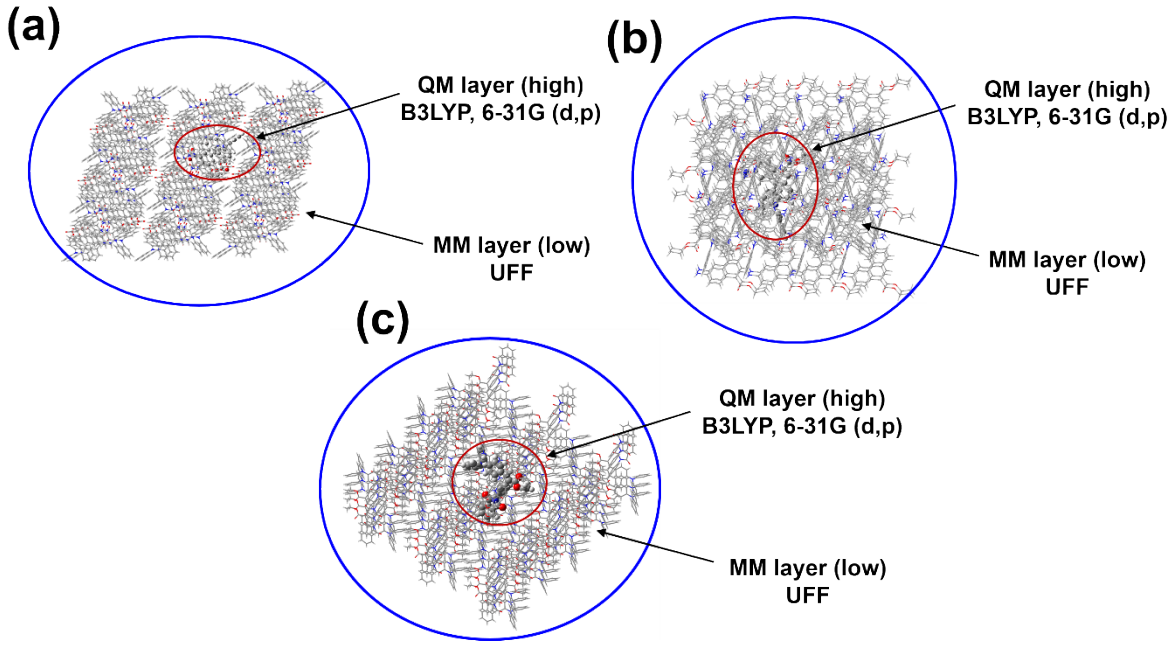

Figure S18. QM and MM layers were chosen from the crystal structure for QM/MM simulations for (a) TN, (b) TA, and (c) TP. For the QM/MM calculation, the QM layer has been treated with B3LYP, 6-31G (d, p) level of theory, while the MM layer has been treated with a classical UFF model of theory.

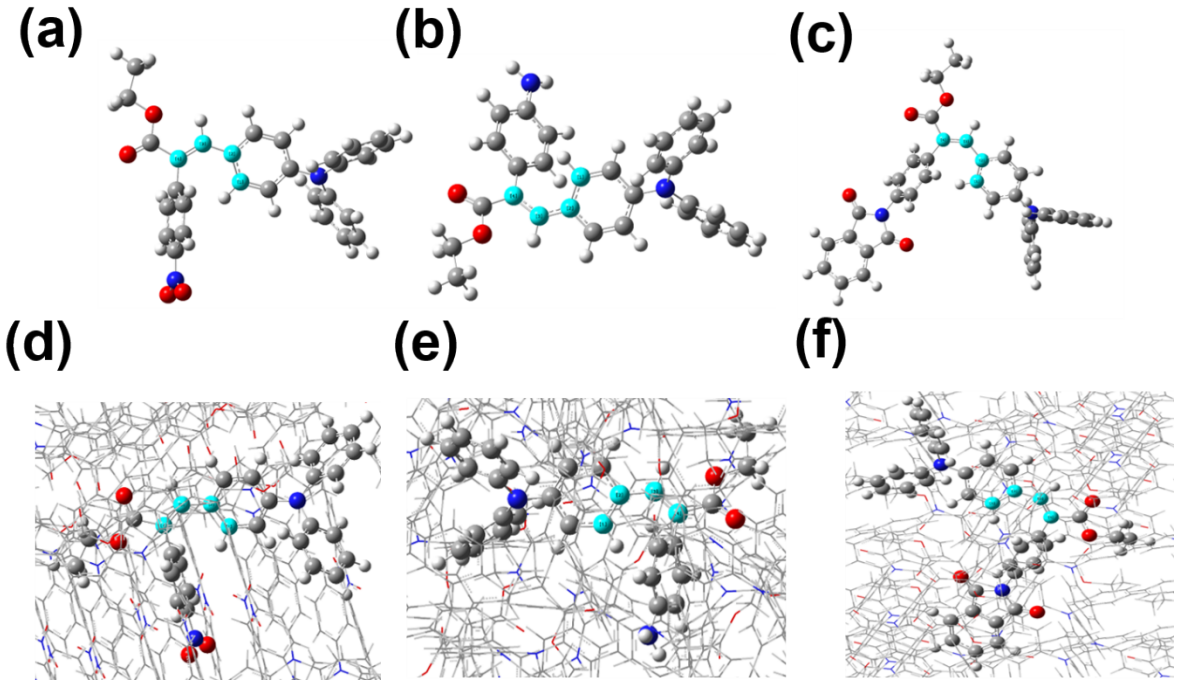

Figure S19. The dihedral angle chosen for Potential energy surface (PES) scanning along (marked in cyan color) for THF-based (a-TN, b-TA, c-TP) and QM/MM-based calculation (d-TN, e-TA, f-TP).

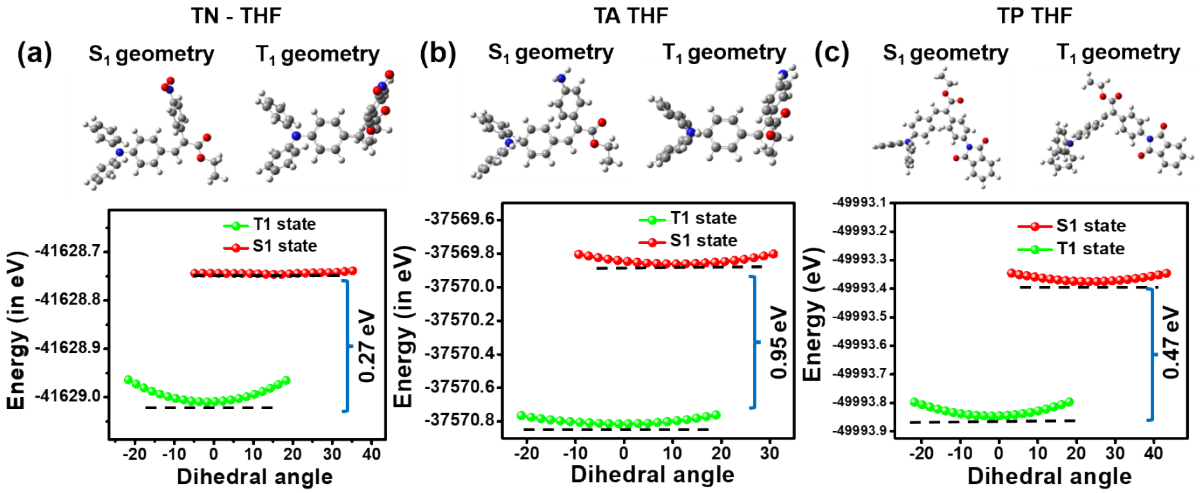

Figure S20. Potential energy scanning along the dihedral angle between donor and acceptor moieties in the solvent phase using the IEFPCM model for (a) TN, (b) TA, and (c) TP. DFT calculations have been performed at B3LYP, 6-31G (d, p) level of theory.

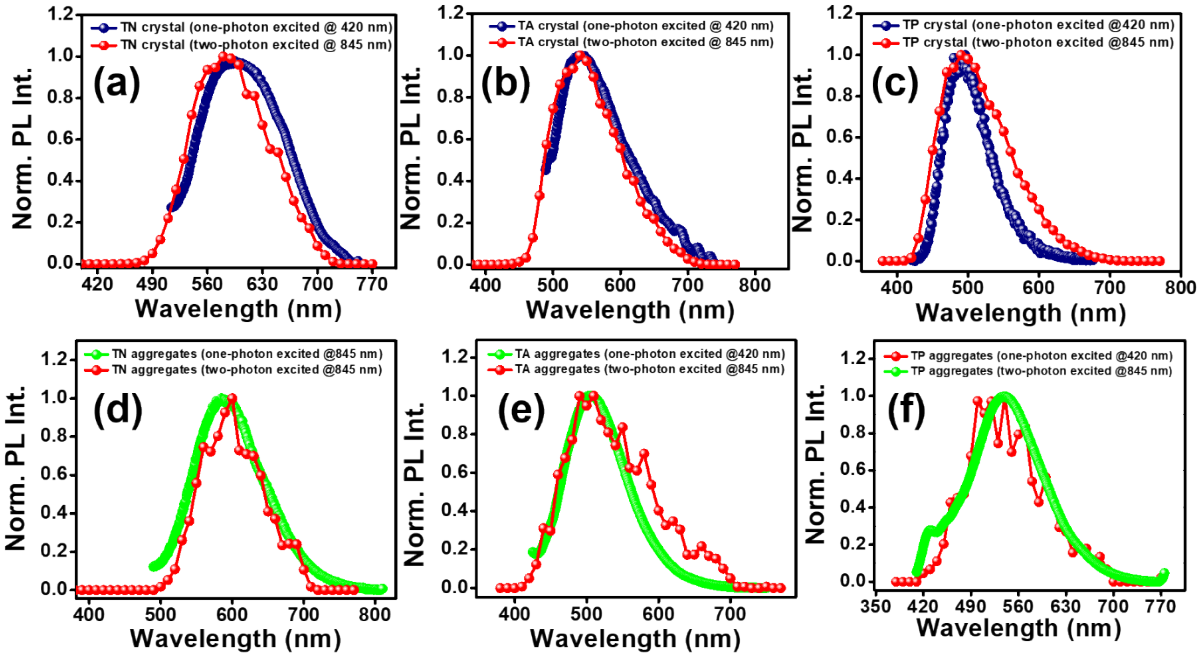

Figure S21. One-photon and two-photon excited emission spectra of the crystals of (a) TN, (b) TA, and (c) TP. One-photon and two-photon excited emission spectra of the molecular aggregates (formed at 95% water- 5% THF binary mixtures) of (d) TN, (e) TA, and (f) TP.

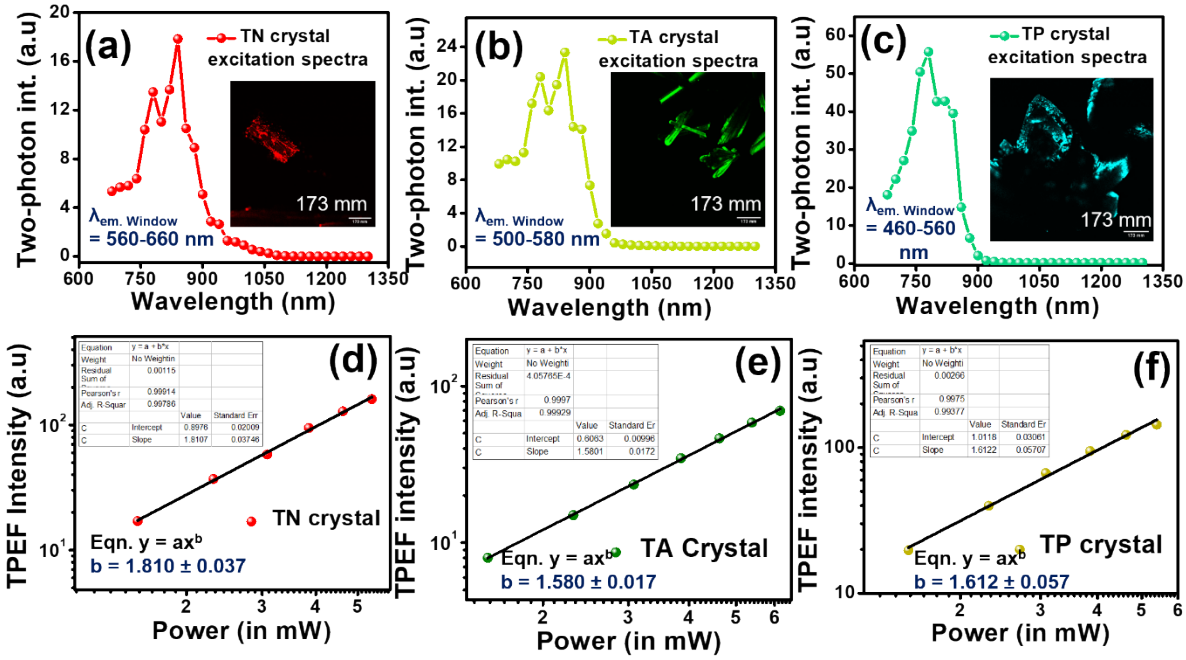

Figure S22. Two-photon excitation spectra for (a) TN (emission range= 560-660 nm), (b) TA (emission range 500-580 nm) and, (c) TP (emission range= 460-560 nm). Excitation power dependent (exc. 845 nm) two-photon excited emission intensity (plotted in log-log scale) for (d) TN, (e) TA and (f) TP.

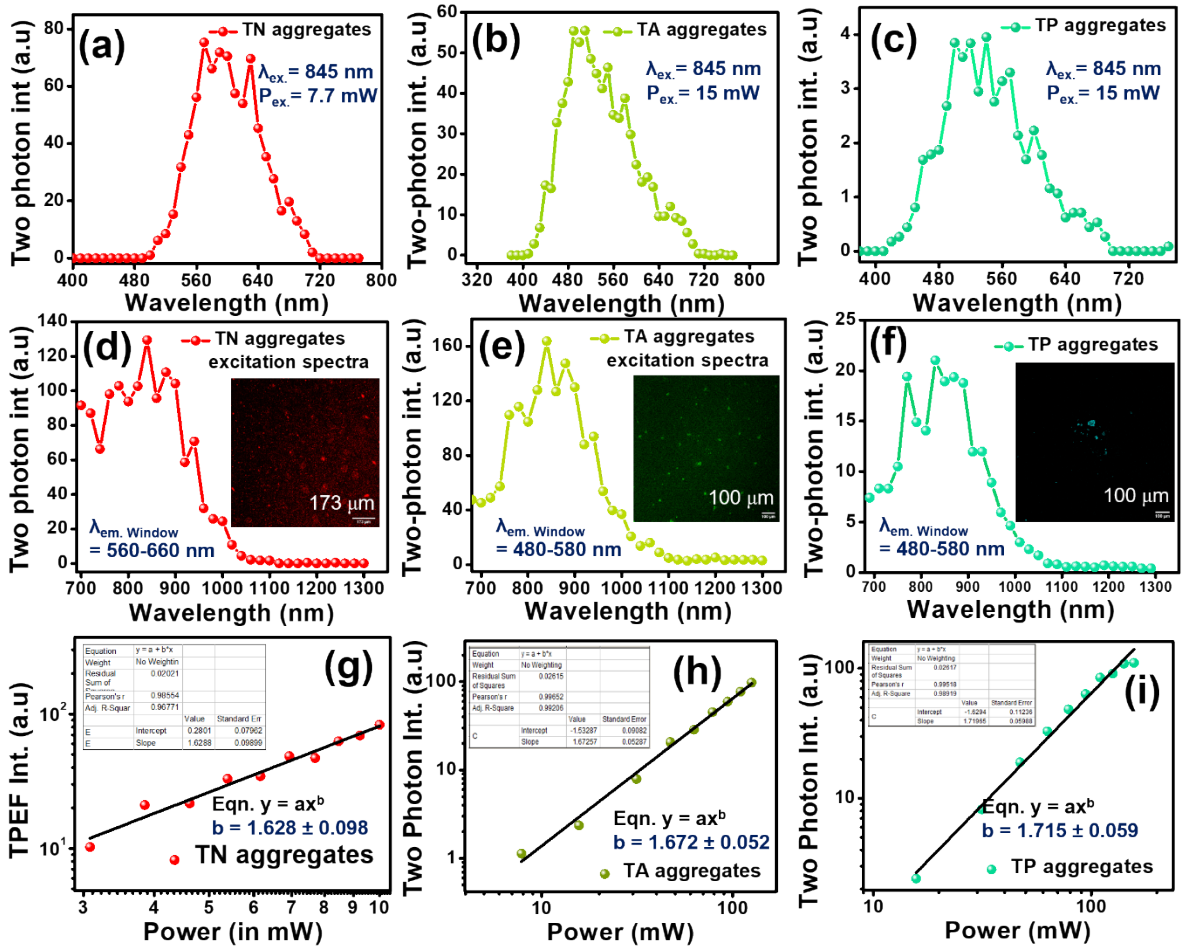

Figure S23. Two-photon excited emission spectra (ex. 845 nm, power= 7.7 mW for TN and 15 mW for TA & TP) of (a) TN, (b) TA, and (c) TP aggregates (formed at 95% water- 5% THF binary mixtures). Two-photon excitation spectra for (d) TN (emission range= 560-660 nm), (e) TA (emission range 480-580 nm), and, (f) TP (emission range= 480-580 nm). Excitation power dependent (ex. 845 nm) two-photon excited emission intensity (plotted in log-log scale) for (g) TN, (h) TA, and (i) TP aggregates.

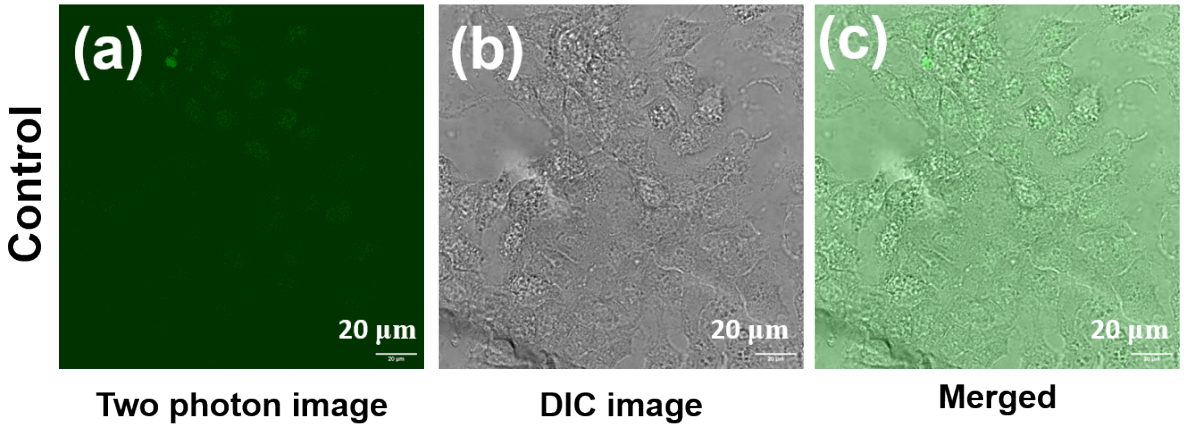

Figure S24. Control experiment for two-photon microscopy imaging of HeLa cells. (a) cells without dye treatment, (b) Differential interference contrast (DIC) image, (c) Merged image of DIC image and cells without dye treatment.

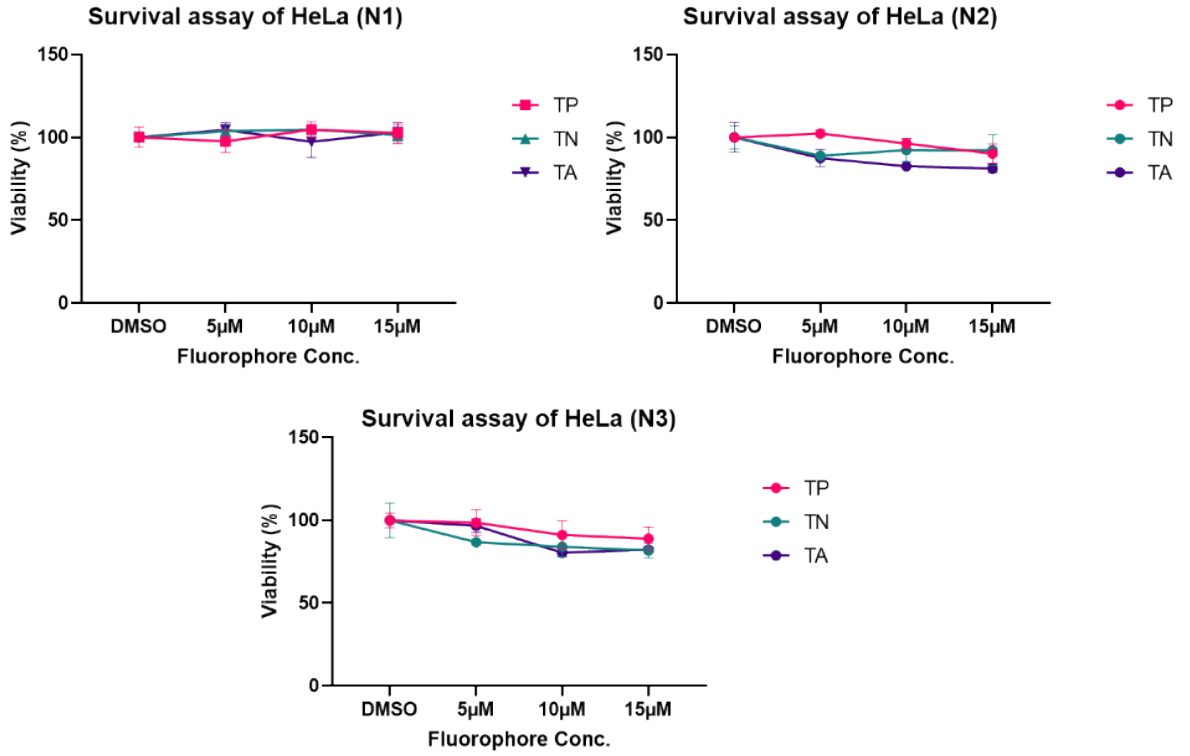

Figure S25. MTT viability assay of HeLa in the presence of different concentrations of dye (TN, TA, and TP) across three biological replicates**.**

Note: Author contribution

AC and PH came up with the idea for the project. AC is the primary contributor in terms of the design, development, execution, and compilation of the project. Synthesis and characterization were performed as a combined effort by AC, SN, ST, and AKS, while ST is the main contributor to HPLC purification of the compounds. Electronic structure calculations were performed by AC and SN, with AC interpreting the theoretical outcomes. AC and SN played a key role in improving the writing and figures for the manuscript. Photophysical measurements were conducted jointly by AC and SN with AC interpreting the outcomes. Two-photon related photophysical measurements were performed by AC. Under the supervision of SBS, AN carried out the experiment for photocurrent generation. AM performed the two-photon cell imaging experiment, and ML supervised it. MDA helped in solving the crystal structures. Revision works have been jointly conducted by AC and MDA. PH supervised the whole project and provided valuable insights throughout its progression.

References

1. (a) Sheldrick, G. M. Acta Crystallogr., Sect. A: Found. Crystallogr. 2008, **64**, 112. (b) Sheldrick, G. M. SHELXL-97, Program for Crystal Structure Solution and Refinement; University of Göttingen: Göttingen, Germany, 1997.

2. Farrugia, L. J. J. Appl. Crystallogr. 1999, **32**, 837.

3. Frisch, M. J.; Trucks, G. W.; Schlegel, H. B.; Scuseria, G. E.; Robb, M. A.; Cheeseman, J. R.; Scalmani, G.; Barone, V.; Mennucci, B.; Petersson, G. A.; et al. Gaussian 09, Revision C.01; Gaussian Inc.: Wallingford, CT, 2009.

4. A. D. Becke, *Phys. Rev. A* 1988, **38**, 3098–3100.

5. C. Lee, W. Yang, R. G. Parr, *Phys. Rev. B* 1988, **37**, 785–789.

6. T. Vreven, K. Morokuma, O. Farkas, H. B. Schlegel, M. J. Frisch, *J. Comput. Chem*. 2003, **24**, 760-769.

7. H. Lin, D. G. Truhlar, *Theor. Chem. Acc*. 2007, **117**, 185-199.

8. A. Chatterjee, J. Chatterjee, S. Sappati, T. Sheikh, R. M. Umesh, M. D. Ambhore, M. Lahiri and P. Hazra, *J. Phys. Chem. B*, 2021, **125**, 12832−12846.

9. Janiak, C. A Critical Account on π−π Stacking in Metal Complexes with Aromatic Nitrogen-Containing Ligands. J. Chem. Soc. Dalt. Trans. 2000, **21**, 3885−3896.

10. Martin, A. D.; Britton, J.; Easun, T. L.; Blake, A. J.; Lewis, W.; Schröder, M. Hirshfeld Surface Investigation of Structure-Directing Interactions within Dipicolinic Acid Derivatives. Cryst. Growth Des. 2015, **15**, 1697–1706.

11. Martin, A. D.; Hartlieb, K. J.; Sobolev, A. N.; Raston, C. L. Hirshfeld Surface Analysis of Substituted Phenols. Cryst. Growth Des. 2010, **10**, 5302–5306.

12. McKinnon, J. J.; Jayatilaka, D.; Spackman, M. A. Towards Quantitative Analysis of Intermolecular Interactions with Hirshfeld Surfaces. Chem. Commun. 2007, **37**, 3814–3816.

13. Spackman, P. R.; Turner, M. J.; McKinnon, J. J.; Wolff, S. K.; Grimwood, D. J.; Jayatilaka, D.; Spackman, M. A. CrystalExplorer: A Program for Hirshfeld Surface Analysis, Visualization and Quantitative Analysis of Molecular Crystals. J. Appl. Crystallogr. 2021, **54**, 1006–1011.

14. Gong, Y.; Chen, G.; Peng, Q.; Yuan, W. Z.; Xie, Y.; Li, S.; Zhang, Y.; Tang, B. Z. Achieving Persistent Room Temperature Phosphorescence and Remarkable Mechanochromism from Pure Organic Luminogens. Adv. Mater. 2015, **27**, 6195−6201.

15. Xie, Z.; Yang, B.; Li, F.; Cheng, G.; Liu, L.; Yang, G.; Xu, H.; Ye, L.; Hanif, M.; Liu, S.; et al. Cross Dipole Stacking in the Crystal of Distyrylbenzene Derivative: The Approach toward High Solid-State Luminescence Efficiency. J. Am. Chem. Soc. 2005, **127**, 14152−14153.

16. Itoh, Y.; Nakashima, Y.; Tsukamoto, S.; Kurohara, T.; Suzuki, M.; Sakae, Y.; Oda, M.; Okamoto, Y.; Suzuki, T. N+-C-H···O Hydrogen Bonds in Protein-Ligand Complexes. Sci. Rep. 2019, **9**, 767.